Optimal Control of Endo-Atmospheric Launch Vehicle Systems: Geometric and Computational Issues

Riccardo Bonalli, Bruno Hérissé and Emmanuel Trélat

Abstract

In this paper we develop a geometric analysis and a numerical method based on indirect methods to solve optimal control problems concerning endo-atmospheric launch vehicle systems. Two main difficulties are addressed. First, the usual approach to restate given mixed control-state constraints as pure control constraints consists in describing the endo-atmospheric flight dynamical model via Euler coordinates which have singularities, and this prevents from solving all reachable configurations. We propose a representation of the configuration manifold with two local charts, in each of which the problem can both be settled in a simpler form and be solved without running into coordinate singularities. Moreover, we prove that no singular arcs arise. The second issue concerns the hard initialization of the indirect method. We introduce a strategy which combines the related shooting method with homotopies, thus providing a high accuracy. For the missile interception problem, our numerical simulations confirm the efficiency of the approach.

Index Terms

Geometric optimal control, Indirect methods, Numerical homotopy methods, Guidance of vehicles.

R. Bonalli is with Onera - The French Aerospace Lab, F-91761 Palaiseau, France, e-mail: riccardo.bonalli@onera.fr

B. Hérissé is with Onera - The French Aerospace Lab, F-91761 Palaiseau, France, e-mail: bruno.herisse@onera.fr

E. Trélat is with Laboratoire Jacques-Louis Lions at Sorbonne Universités, UPMC Univ Paris 06, CNRS UMR 7598, F-75005, Paris, France, e-mail: emmanuel.trelat@upmc.fr

I. Introduction

A. Optimal Guidance of Launch Vehicle Systems

Guidance of autonomous launch vehicles towards rendezvous points is a complex task often considered in aerospace applications. It can be modeled as an optimal control problem, with the objective of finding a control law enabling the vehicle to join a final point considering prescribed constraints as well as performance criteria. The rendezvous point may be a static point as well as a moving point if, for example, the mission consists in reaching a maneuvering target. Then, an important challenge consists in developing analysis and algorithms able to provide *high numerical precision* of optimal trajectories, considering rough onboard processors, that is with low computational capability.

In the engineering community, one of the most widespread approaches to solve this kind of task resides on *analytical guidance laws* (see, e.g. [25], [26], [37], [29], [22]). They correct errors coming from perturbations and misreading of the system. Nonetheless, the trajectories induced by guidance laws are usually not optimal because of some considered approximations. On the other hand, ensuring the optimality of trajectories can be achieved rather exploiting *direct methods* (see, e.g. [19], [35], [36], [31], [39]). These techniques consist in discretizing each component of the optimal control problem (the state, the control, etc.) to reduce it to a nonlinear constrained optimization problem. A high degree of robustness is provided while, in general, no deep knowledge of the dynamical system is required, making these methods rather easy to use in practice. However, their efficiency is proportional to the computational load which often obliges to use them offline.

Good candidates to manage efficiently an onboard processing of optimal trajectories are *indirect methods* (see, e.g. [10], [11], [27], [30], [32]). Necessary conditions coming from the *Pontryagin Maximum Principle* (PMP) (see [33], [24]) wrap the optimal guidance system into a two-point boundary value problem, leading to accurate and fast algorithms. The advantages of indirect methods, whose more basic version is known as *shooting method*, are their extremely good numerical accuracy and the fact that, if they converge, the convergence is very quick. Nevertheless, treating *mixed control-state constraints* with necessary conditions and *initializing* indirect methods still remain challenging.

B. Mixed Control-State Constraints and Euler Singularities

An accurate study of the optimal guidance of launch vehicles compels to consider both usually demanding performance criteria and possible onerous missions to accomplish. Since, in this situation, the vehicle is subject to several strong mechanical strains, some stability constraints must be imposed, which turn out to be modeled as mixed control-state constraints. This kind of optimal control problems is more difficult to treat by the Maximum Principle (see, e.g. [8], [20], [15], [13]). Indeed, further Lagrange multipliers appear, for which, obtaining rigorous and useful information may be arduous and has been the object of many studies in the existing literature (see, e.g. [23], [28], [7], [6], [2]).

A widespread approach in aeronautics to avoid to deal with these particular mixed control-state constraints consists in reformulating the original guidance problem using some *local Euler coordinates*, under which, the structural constraints become pure control constraints (see for example [7], [34]; we report this change of coordinates in Section III-B). The transformation allows to consider the standard Maximum Principle and, then, usual shooting methods. However, Euler coordinates are not global and have singularities that prevent from solving all reachable configurations, reducing the number of possible achievable missions.

We fix this issue by reformulating the optimal guidance problem within an intrinsic viewpoint, using geometric control (and it does not seem that this general framework has been systematically investigated in the optimal guidance context so far). In particular, we build additional local coordinates which cover the singularities of the previous ones and under which the mixed control-state constraints can be still reinterpreted as pure control constraints. Moreover, these two sets of local coordinates form an atlas of the configuration manifold and can be exploited to recover completely the behavior of optimal controls even if there are some singular arcs.

We stress on the fact that the introduction of these particular local coordinates provides, in turn, two main benefits. On one hand, there is no limit on the feasible mission scenarios that can be simulated, and, on the other hand, the optimal guidance problem is not conditioned by multipliers depending on mixed constraints (or, at least, locally), then, standard shooting or multi-shooting methods can be easily put in practice. This is at the price of changing chart (local coordinates), which complicates a bit the implementation of the shooting method, but, importantly, does not affect its efficiency.

C. Our Numerical Approach and Applications

The main advantage of indirect methods is their extremely good numerical accuracy. Indeed, since they rely on the Newton method, they inherit of the very quick convergence properties of the Newton method. Nevertheless, it is known that their main drawback is related to their initialization. This issue can be addressed by *homotopy methods* (we refer to [1] for classical frameworks).

The basic idea of homotopy methods is to solve a difficult problem step by step starting from a simpler problem (that we call *problem of order zero*) by parameter deformation. Combined with the shooting problem derived from the Maximum Principle, a homotopy method consists in deforming the problem into a simpler one (which can be easily solved) and then solving a series of shooting problems step by step to come back to the original problem. In the case in which the homotopic parameter is a real number and when the path consists in a convex combination of the problem of order zero and of the original problem, the homotopy method is rather called a *continuation method*.

Homotopy procedures have proved to be reliable and robust for problems in the aerospace context like orbit transfer, atmospheric reentry and planar tilting maneuvers (see, e.g. [12], [18], [40], [41]). Here, we propose a numerical homotopy scheme to solve the shooting problem coming from the optimal guidance framework, ensuring a high numerical accuracy of optimal trajectories.

In order to practically apply this homotopy algorithm, we give numerical solutions of the *endo-atmospheric missile interception* problem (presented, for example, in [14]). We are able to provide a problem of order zero which is a good candidate to initialize the first homotopic iterations. Then, we can recover the optimal solution of the original problem by a linear continuation method, ensuring the convergence of the whole algorithm.

D. Structure of the Paper

The paper is organized as follows. Section II contains details on the model under consideration and the optimal problem statement. Sections III-A, III-B and III-D are devoted repectively to the Maximum Principle formulation, its intrinsic geometric behavior analysis and the computations of the optimal controls as functions of the state and the costate. Singular controls are analyzed too. In Sections IV and V we provide the numerical scheme, giving a complete numerical solution

of the endo-atmospheric missile interception problem. Finally, Section VI contains conclusions and perspectives.

II. Optimal Guidance Problem

A. Model Dynamics

We focus on a class of launch vehicles modeled as a three-dimensional axial symmetric cylinder, where $\boldsymbol{u}$ denotes its principal body axis, steered by a control system (based on steering fins or a Reaction Control System for example). We denote by Q the point of the vehicle where this system is placed. Let O be the center of the Earth, $\boldsymbol{K}$ be the northsouth axis of the planet and consider an orthonormal inertial frame $(\boldsymbol{I}, \boldsymbol{J}, \boldsymbol{K})$ centered at O. For the applications presented, the effect of the rotation of the Earth can be neglected. The motion of the vehicle, denoting with G its center of mass, is described by the state variables $(\boldsymbol{r}(t), \boldsymbol{v}(t), \boldsymbol{u}(t))$, where $\boldsymbol{r}(t) = x(t)\boldsymbol{I} + y(t)\boldsymbol{J} + z(t)\boldsymbol{K}$ is the trajectory of G while $\boldsymbol{v}(t) = \dot{x}(t)\boldsymbol{I} + \dot{y}(t)\boldsymbol{J} + \dot{z}(t)\boldsymbol{K}$ is its velocity.

We denote by P the center of pressure, by m the mass of the vehicle, by $\rho(\boldsymbol{r})$ the air density (a standard exponential law of type $\rho_0 \exp(-(\|\boldsymbol{r}\| - r_T)/h_r)$ is considered, where $\rho_0 > 0$, r_T is the radius of the Earth and h_r is a reference altitude) and by S a constant reference surface for aerodynamical forces. Then, the forces and torques applied to the vehicle are:

- the gravity $\boldsymbol{g} = -g(\boldsymbol{r})\frac{\boldsymbol{r}}{\|\boldsymbol{r}\|}$, acting at G;
- the drag $\boldsymbol{D} = -\frac{1}{2}\rho(\boldsymbol{r})SC_D\|\boldsymbol{v}\|\boldsymbol{v}$, acting at P, where $C_D = C_{D_0} + C_{D_1}\left(\frac{\|\boldsymbol{u}\wedge\boldsymbol{v}\|}{\|\boldsymbol{v}\|}\right)^2$ is a quadratic approximation of the drag coefficient (C_{D_0}, C_{D_1} are positive constants);
- the lift $\boldsymbol{L} = \frac{1}{2}\rho(\boldsymbol{r})SC_{L_\alpha}\big(\boldsymbol{v}\wedge(\boldsymbol{u}\wedge\boldsymbol{v})\big)$, acting at P, where the coefficient C_{L_α} is considered constant;
- the thrust $\boldsymbol{T} = f_T(t)\boldsymbol{u}$, acting at Q, where $f_T(t)$ is nonnegative and proportional to the mass flow $q(t)$;
- the skid-to-turn force $\boldsymbol{W}$, acting at Q, which includes the aerodynamical contribution due to the control system;
- the overturning torque $\boldsymbol{M} = \frac{1}{2}\rho(\boldsymbol{r})SC_L\|\boldsymbol{v}\|\frac{\boldsymbol{v}\wedge\boldsymbol{GP}}{\|GP\|}$ which includes the turning components of drag and lift.

Structural optimization ensures that torques do not affect the dynamics of the momentum. As a standard result (see, e.g. [34]), the following rigid body dynamics is obtained

$$\begin{cases} \dot{\boldsymbol{r}}(t) = \boldsymbol{v}(t) \ , \ \dfrac{d}{dt}(I_G\boldsymbol{\omega})(t) = -\boldsymbol{\omega}(t) \wedge I_G(t)\boldsymbol{\omega}(t) + \dfrac{\boldsymbol{W} \wedge \boldsymbol{GQ}}{\|GQ\|} + \boldsymbol{M} \\ \dot{\boldsymbol{v}}(t) = \boldsymbol{f}(t, \boldsymbol{r}(t), \boldsymbol{v}(t), \boldsymbol{u}(t)) := \\ \dfrac{\boldsymbol{T}(t, \boldsymbol{u}(t))}{m(t)} + \boldsymbol{g}(\boldsymbol{r}(t)) + \dfrac{\boldsymbol{D}(\boldsymbol{r}(t), \boldsymbol{v}(t), \boldsymbol{u}(t))}{m(t)} + \dfrac{\boldsymbol{L}(\boldsymbol{r}(t), \boldsymbol{v}(t), \boldsymbol{u}(t))}{m(t)} \end{cases} \tag{1}$$

where $I_G(t)$ denotes the inertial matrix of the vehicle at G while $\boldsymbol{\omega}(t)$ denotes its angular velocity in body axis at time t. Since the evolution of the mass flow $q(t)$ is known a priori, the evolutions of $I_G(t)$ and $m(t)$ are known as well.

Remark 1: The principal body axis $\boldsymbol{u}$ is a function of the angular velocity $\boldsymbol{\omega}$. Moreover, some stability constraints naturally appear. In particular, the velocity is always positively oriented w.r.t. the principal body axis and, to stabilize the vehicle, it is recommended to force the velocity $\boldsymbol{v}(t)$ such that its values are inside a cone around the body axis $\boldsymbol{u}(t)$, of maximal amplitude $0 < \alpha_{\max} \leq \pi/6$ ($\alpha_{\max}$ is the *maximal angle of attack*). In this paper, we do not consider structural limits such as the *load factor*. It is not difficult to extend our results if these limits are considerd (following Section IV).

At this stage, (1) represents a control system on which one can act on $\boldsymbol{W}$. More specifically, system (1) means the dynamics of a *guidance and control of launch vehicle systems problem.*

B. General Optimal Guidance Problem

In practical applications, rotational dynamics are faster than traslational dynamics. Then, it is more convenient to divide and treat separately respectively the *guidance system* and the *control system*.

The computation of an optimal strategy concerns the guidance system only. Then, we can simplify system (1) into

$$\begin{cases} \dot{\boldsymbol{r}}(t) = \boldsymbol{v}(t) \quad , \quad \dot{\boldsymbol{v}}(t) = \boldsymbol{f}(t, \boldsymbol{r}(t), \boldsymbol{v}(t), \boldsymbol{u}(t)) \\ (\boldsymbol{r}(t), \boldsymbol{v}(t)) \in N \quad , \quad \boldsymbol{u}(t) \in S^2 \quad , \quad (\boldsymbol{r}(T), \boldsymbol{v}(T)) \in M \subseteq N \\ c_1(\boldsymbol{v}(t), \boldsymbol{u}(t)) := -\boldsymbol{v}(t) \cdot \boldsymbol{u}(t) \leq 0 \quad , \quad \boldsymbol{r}(0) = \boldsymbol{r}_0 \ , \ \boldsymbol{v}(0) = \boldsymbol{v}_0 \\ c_2(\boldsymbol{v}(t), \boldsymbol{u}(t)) := \left(\dfrac{\|\boldsymbol{u}(t) \wedge \boldsymbol{v}(t)\|}{\|\boldsymbol{v}(t)\| \sin \alpha_{\max}} \right)^2 - 1 \leq 0 \end{cases} \tag{2}$$

where N is an open subset of $\mathbb{R}^6 \setminus \{0\}$ consisting of all possible scenarios (see Remark 2 in Section III-B), $(\boldsymbol{r}_0, \boldsymbol{v}_0) \in N$ are given intial values, M is a subset of N and, now, the control variable becomes the principal body axis $\boldsymbol{u}$.

In this general context, a mission depends on which kind of launch vehicle we treat and which specific task it has to accomplish. Then, for the moment, we do not make precise neither the cost nor the set M of final conditions, saying that our General Optimal Guidance Problem (**GOGP**) consists in minimizing the cost function

$$C_T(\boldsymbol{r}(\cdot), \boldsymbol{v}(\cdot), \boldsymbol{u}(\cdot)) = g(T, \boldsymbol{r}(T), \boldsymbol{v}(T))$$

under the dynamical control system (2), where g is of class C^1 and the final time T may be free or not. Nevertheless, the computations of the optimal control using an indirect method framework cannot be totally accomplished (see Section III-D) unless considering further assumptions on g and M. In particular we suppose the following:

Assumption 1: The set M is a submanifold of N and satisfies at least one between the following two conditions:

A) The final time T is free and $\dfrac{\partial g}{\partial t}(T, \boldsymbol{r}, \boldsymbol{v}) \neq 0$;

B) It holds $M = \Big\{(\boldsymbol{r}, \boldsymbol{v}) \in N : F(\boldsymbol{r}, \boldsymbol{v}) = 0\Big\}$, where F is a smooth submersion. Moreover, for every local chart $(x_1, \ldots, x_6)(\boldsymbol{r}, \boldsymbol{v})$ of N, there always exists a free final variable, let say x_i, such that $\frac{\partial g}{\partial x_i}(T, \boldsymbol{r}, \boldsymbol{v}) \neq 0$.

III. Maximum Principle and Optimal Synthesis in the Two Charts

A. Maximum Principle for Mixed Control-State Constraints

In (2) we have two mixed control-state constraints c_1 and c_2. Let $(\boldsymbol{r}(\cdot), \boldsymbol{v}(\cdot), \boldsymbol{u}(\cdot))$ be optimal for (**GOGP**), with final time T. Since $c_2(\boldsymbol{v}, \boldsymbol{u})$ forces $c_1(\boldsymbol{v}, \boldsymbol{u})$ to be negative, we take into account only the following strong regularity assumption

$$\text{rank} \begin{pmatrix} \partial_{u_1} c_2 & \partial_{u_2} c_2 & \partial_{u_3} c_2 \end{pmatrix} (\boldsymbol{v}, \boldsymbol{u}) = 1$$

for points such that $c_2(\boldsymbol{v}, \boldsymbol{u}) \geq 0$, which is always satisfied. We denote $\boldsymbol{p} = (\boldsymbol{p}_1, \boldsymbol{p}_2) \in \mathbb{R}^3 \times \mathbb{R}^3$ and define by

$$\begin{aligned} H(t, \boldsymbol{r}, \boldsymbol{v}, \boldsymbol{p}, \mu_1, \mu_2, \boldsymbol{u}) &= H^0(t, \boldsymbol{r}, \boldsymbol{v}, \boldsymbol{p}, \boldsymbol{u}) + \mu_1 c_1(\boldsymbol{v}, \boldsymbol{u}) + \mu_2 c_2(\boldsymbol{v}, \boldsymbol{u}) \\ &= \langle \boldsymbol{p}_1, \boldsymbol{v} \rangle + \langle \boldsymbol{p}_2, \boldsymbol{f}(t, \boldsymbol{r}, \boldsymbol{v}, \boldsymbol{u}) \rangle + \mu_1 c_1(\boldsymbol{v}, \boldsymbol{u}) + \mu_2 c_2(\boldsymbol{v}, \boldsymbol{u}) \end{aligned} \tag{3}$$

the *Hamiltonian* of (**GOGP**). According to the Maximum Principle (see, e.g. [33], [21]), there exist, under appropriate identifications, a non-positive scalar p^0, an absolutely continuous mapping $\boldsymbol{p} : [0,T] \to T^*N \simeq \mathbb{R}^6$ called *adjoint vector* and functions $\mu_1(\cdot), \mu_2(\cdot) \in L^\infty([0,T],\mathbb{R})$, with $(\boldsymbol{p}(\cdot), p^0) \neq 0$, such that the so-called *extremal* $(\boldsymbol{r}(\cdot), \boldsymbol{v}(\cdot), \boldsymbol{p}(\cdot), p^0, \mu_1(\cdot), \mu_2(\cdot), \boldsymbol{u}(\cdot))$ satisfies a.e. in $[0,T]$:

- **Adjoint Equations**

$$\begin{cases} \begin{pmatrix} \dot{\boldsymbol{r}}(t) \\ \dot{\boldsymbol{v}}(t) \end{pmatrix} = \dfrac{\partial H}{\partial \boldsymbol{p}}(t, \boldsymbol{r}(t), \boldsymbol{v}(t), \boldsymbol{p}(t), \mu_1(t), \mu_2(t), \boldsymbol{u}(t)) \\ \dot{\boldsymbol{p}}(t) = -\dfrac{\partial H}{\partial(\boldsymbol{r}, \boldsymbol{v})}(t, \boldsymbol{r}(t), \boldsymbol{v}(t), \boldsymbol{p}(t), \mu_1(t), \mu_2(t), \boldsymbol{u}(t)) \end{cases} \tag{4}$$

- **Maximality Conditions**

$$H^0(t, \boldsymbol{r}(t), \boldsymbol{v}(t), \boldsymbol{p}(t), \boldsymbol{u}(t)) \geq H^0(t, \boldsymbol{r}(t), \boldsymbol{v}(t), \boldsymbol{p}(t), \boldsymbol{u}) \tag{5}$$

$$\text{for every } \boldsymbol{u} \text{ such that: } \boldsymbol{u} \in S^2 \ , \ c_1(\boldsymbol{v}(t), \boldsymbol{u}) \leq 0 \ , \ c_2(\boldsymbol{v}(t), \boldsymbol{u}) \leq 0$$

$$\frac{\partial H}{\partial \boldsymbol{u}}(t, \boldsymbol{r}(t), \boldsymbol{v}(t), \boldsymbol{p}(t), \mu_1(t), \mu_2(t), \boldsymbol{u}(t)) = 0 \tag{6}$$

- **Complementarity Slackness Conditions**

$$\begin{cases} \mu_1(t) c_1(\boldsymbol{v}(t), \boldsymbol{u}(t)) = 0 \\ \mu_2(t) c_2(\boldsymbol{v}(t), \boldsymbol{u}(t)) = 0 \end{cases} \ , \ \mu_1(t) \leq 0 \ , \ \mu_2(t) \leq 0 \tag{7}$$

- **Transversality Conditions**

$$\boldsymbol{p}(T) - p^0 \frac{\partial g}{\partial(\boldsymbol{r}, \boldsymbol{v})}(T, \boldsymbol{r}(T), \boldsymbol{v}(T)) \perp T_{(\boldsymbol{r}(T), \boldsymbol{v}(T))} M \tag{8}$$

  Moreover, if the final time T is free, then

$$\max_{\boldsymbol{u}} H^0(T, \boldsymbol{r}(T), \boldsymbol{v}(T), \boldsymbol{p}(T), \boldsymbol{u}) = -p^0 \frac{\partial g}{\partial t}(T, \boldsymbol{r}(T), \boldsymbol{v}(T)) \tag{9}$$

$$\text{and the } \max \text{ is taken on: } \boldsymbol{u} \in S^2 \ , \ c_1(\boldsymbol{v}(T), \boldsymbol{u}) \leq 0 \ , \ c_2(\boldsymbol{v}(T), \boldsymbol{u}) \leq 0$$

The extremal is said *normal* if $p^0 \neq 0$ and, in this case, it is usual to set $p^0 = -1$. Otherwise, the extremal is said *abnormal*. As we pointed out previously, obtaining rigorous and useful information on the multipliers $\mu_1(\cdot)$, $\mu_2(\cdot)$ may be difficult, which consequently makes challenging applying indirect methods.

In this situation, a change of coordinates, which is commonly used in aerospace applications, can be performed to transform the mixed control-state constraints c_1 and c_2 into pure control

constraints, allowing to use standard shooting methods. However, this transformation acts only locally, preventing from representing the whole configuration manifold N. For sake of clarity, we first recall this standard transformation, and then, we show how to fix the presence of Euler singularities by introducing further coordinates, in which, c_1 and c_2 still become pure control constraints.

B. Local Model with Respect to Two Charts

1) Reduction to Pure Control Constraints via Local Coordinates: We denote by (r, L, ℓ) the spherical coordinates of the center of mass G of the vehicle w.r.t. $(\boldsymbol{I}, \boldsymbol{J}, \boldsymbol{K})$, where r is the distance OG, L the latitude and ℓ the longitude. We denote $(\boldsymbol{e}_L, \boldsymbol{e}_\ell, \boldsymbol{e}_r)$ the *North-East-Down* (NED) frame, a moving frame centered at G, where $-\boldsymbol{e}_r$ is the local vertical direction, $(\boldsymbol{e}_L, \boldsymbol{e}_\ell)$ is the local horizontal plane while $\boldsymbol{e}_L$ is pointing to the North. By definition

$$\begin{cases} \boldsymbol{e}_L = -\sin(L)\cos(\ell)\boldsymbol{I} - \sin(L)\sin(\ell)\boldsymbol{J} + \cos(L)\boldsymbol{K} \\ \boldsymbol{e}_\ell = -\sin(\ell)\boldsymbol{I} + \cos(\ell)\boldsymbol{J} \\ \boldsymbol{e}_r = -\cos(L)\cos(\ell)\boldsymbol{I} - \cos(L)\sin(\ell)\boldsymbol{J} - \sin(L)\boldsymbol{K} \end{cases}$$

for which $\boldsymbol{r} = -r\boldsymbol{e}_r$ and it is straightforward to have

$$\dot{\boldsymbol{e}}_L = -\dot{\ell}\sin(L)\boldsymbol{e}_\ell + \dot{L}\boldsymbol{e}_r \ , \ \dot{\boldsymbol{e}}_\ell = \dot{\ell}\sin(L)\boldsymbol{e}_L + \dot{\ell}\cos(L)\boldsymbol{e}_r \tag{10}$$

$$\dot{\boldsymbol{e}}_r = -\dot{L}\boldsymbol{e}_L - \dot{\ell}\cos(L)\boldsymbol{e}_\ell$$

Then, the transformation from the frame $(\boldsymbol{I}, \boldsymbol{J}, \boldsymbol{K})$ to the frame $(\boldsymbol{e}_L, \boldsymbol{e}_\ell, \boldsymbol{e}_r)$ is

$$R(L,\ell) := \begin{pmatrix} -\sin(L)\cos(\ell) & -\sin(L)\sin(\ell) & \cos(L) \\ -\sin(\ell) & \cos(\ell) & 0 \\ -\cos(L)\cos(\ell) & -\cos(L)\sin(\ell) & -\sin(L) \end{pmatrix} \in SO(3)$$

To obtain c_1 and c_2 as pure control constraints, further coordinates for the velocity must be introduced. Using the classical formulation in the azimuth/path angle coordinates (see, e.g. [7]), we introduce the *first velocity frame* $(\boldsymbol{i}_1, \boldsymbol{j}_1, \boldsymbol{k}_1)$:

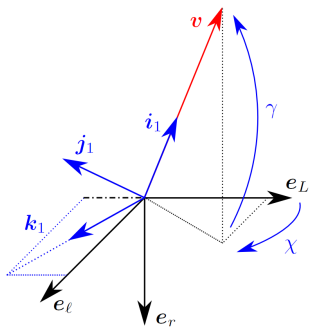

Fig. 1. Frame $(\boldsymbol{i}_1, \boldsymbol{j}_1, \boldsymbol{k}_1)$.

$$\begin{cases} \boldsymbol{i}_1 := \dfrac{\boldsymbol{v}}{v} = \cos(\gamma)\cos(\chi)\boldsymbol{e}_L + \cos(\gamma)\sin(\chi)\boldsymbol{e}_\ell - \sin(\gamma)\boldsymbol{e}_r \\ \boldsymbol{j}_1 := -\sin(\gamma)\cos(\chi)\boldsymbol{e}_L - \sin(\gamma)\sin(\chi)\boldsymbol{e}_\ell - \cos(\gamma)\boldsymbol{e}_r \\ \boldsymbol{k}_1 := -\sin(\chi)\boldsymbol{e}_L + \cos(\chi)\boldsymbol{e}_\ell \end{cases} \tag{11}$$

where $v = \|\boldsymbol{v}\|$. The rotation from the frame $(\boldsymbol{e}_L, \boldsymbol{e}_\ell, \boldsymbol{e}_r)$ to the frame $(\boldsymbol{i}_1, \boldsymbol{j}_1, \boldsymbol{k}_1)$ is then

$$R_a(\gamma,\chi) = \begin{pmatrix} \cos(\gamma)\cos(\chi) & \cos(\gamma)\sin(\chi) & -\sin(\gamma) \\ -\sin(\gamma)\cos(\chi) & -\sin(\gamma)\sin(\chi) & -\cos(\gamma) \\ -\sin(\chi) & \cos(\chi) & 0 \end{pmatrix} \in SO(3)$$

It is important to note that $(r, L, \ell, v, \gamma, \chi)$ represent local coordinates for the dynamics of (**GOGP**) i.e., there exists a local chart of $\mathbb{R}^6 \setminus \{0\}$ whose coordinates are exactly $(r, L, \ell, v, \gamma, \chi)$. Indeed, denote $U = \left[(0,\infty)\times\left(-\frac{\pi}{2},\frac{\pi}{2}\right)\times(-\pi,\pi)\right]^2$ and define the mapping $\varphi_a^{-1} : U \longrightarrow \mathbb{R}^6\setminus\{0\}$ such that

$$\varphi_a^{-1}(r, L, \ell, v, \gamma, \chi) = \Bigg(r\cos(L)\cos(\ell), r\cos(L)\sin(\ell), \tag{12}$$

$$r\sin(L), R^T(L,\ell)\cdot R_a^T(\gamma,\chi)\begin{pmatrix} v \\ 0 \\ 0 \end{pmatrix}\Bigg)$$

this mapping is an injective embedding, hence its inverse is a local chart (in the sense of differential geometry) with respect to $U_a := \varphi_a^{-1}(U)$ which is an open subset of $\mathbb{R}^6 \setminus \{0\}$. Exploiting (10) and the definition of $(\boldsymbol{i}_1, \boldsymbol{j}_1, \boldsymbol{k}_1)$, in the coordinates provided by (12), the derivative of $\boldsymbol{v}$ is

$$\dot{\boldsymbol{v}} = \dot{v}\boldsymbol{i}_1 + \left(v\dot{\gamma} - \frac{v^2}{r}\cos(\gamma)\right)\boldsymbol{j}_1 + \tag{13}$$

$$\left(v\cos(\gamma)\dot{\chi} - \frac{v^2}{r}\cos^2(\gamma)\sin(\chi)\tan(L)\right)\boldsymbol{k}_1 \ .$$

As a final step, we introduce new control variables (which are functions of the original control $\boldsymbol{u}$), under which, c_1 and c_2 can be reformulated as pure control constraints. For this, define the new control $\boldsymbol{w} = R_a(\gamma,\chi)\cdot R(L,\ell)\boldsymbol{u}$. Then, the constraint functions become (by using the fact that $v > 0$)

$$c_1(\boldsymbol{w}) = -w_1 \quad , \quad c_2(\boldsymbol{w}) = \frac{w_2^2 + w_3^2}{\sin^2(\alpha_{\max})} - 1 \quad , \quad \boldsymbol{w} \in S^2 \tag{14}$$

which are pure control constraints. Then, introducing the normalized drag and lift coefficients $d = \frac{1}{2m}\rho S C_{D_0}$, $c_m = \frac{1}{2m}\rho S C_{L_\alpha}$, denoting by $\eta > 0$ the efficiency factor and $\omega(t) = \frac{f_T(t)}{m(t)v(t)} +$

$v(t)c_m(t) > 0$, with the help of (13), the local evaluation of the dynamics of system (1) using the chart φ_a gives

$$\begin{cases} \dot{r} = v\sin(\gamma)\ ,\ \dot{L} = \dfrac{v}{r}\cos(\gamma)\cos(\chi)\ ,\ \dot{\ell} = \dfrac{v}{r}\dfrac{\cos(\gamma)\sin(\chi)}{\cos(L)} \\ \dot{v} = \dfrac{f_T}{m}w_1 - \left(d + \eta c_m(w_2^2 + w_3^2)\right)v^2 - g\sin(\gamma) \\ \dot{\gamma} = \omega w_2 + \left(\dfrac{v}{r} - \dfrac{g}{v}\right)\cos(\gamma) \\ \dot{\chi} = \dfrac{\omega}{\cos(\gamma)}w_3 + \dfrac{v}{r}\cos(\gamma)\sin(\chi)\tan(L) \end{cases} \tag{15}$$

The previous computations allow to reformulate (**GOGP**) introducing a new control problem, named (**GOGP**)$_a$, which consists in minimizing the cost

$$C_T^a(r, L, \ell, v, \gamma, \chi, \boldsymbol{w}) = g(T, \varphi_a^{-1}(r, L, \ell, v, \gamma, \chi)(T))$$

subject to the dynamics (15) and the control constraints (14). This pure control constraint optimal control problem is locally equivalent to (**GOGP**).

Even if formulation (**GOGP**)$_a$ is widely used in the aerospace community, it does not allow to describe totally the original problem (**GOGP**) because of its local nature. Indeed, in several situations, demanding performance criteria C_T and onerous missions force optimal trajectories to pass through points that do not lie within the domain of the local chart φ_a, and then, exploiting (**GOGP**)$_a$ either the optimality could be lost or, in the worst case, the numerical computations may fail.

2) Additional Coordinates to Manage Eulerian Singularities: We introduce another set of coordinates which cover the singularities (with respect to the path angle γ) of chart (U_a, φ_a) in which the constraints c_1 and c_2 are pure control constraints, as provided by expressions (14).

Define the *second velocity frame* $(\boldsymbol{i}_2, \boldsymbol{j}_2, \boldsymbol{k}_2)$ by

$$\begin{cases} \boldsymbol{i}_2 = \dfrac{\boldsymbol{v}}{\|\boldsymbol{v}\|} = \cos(\theta)\sin(\phi)\boldsymbol{e}_L + \sin(\theta)\boldsymbol{e}_\ell + \cos(\theta)\cos(\phi)\boldsymbol{e}_r \\ \boldsymbol{j}_2 = -\sin(\theta)\sin(\phi)\boldsymbol{e}_L + \cos(\theta)\boldsymbol{e}_\ell - \sin(\theta)\cos(\phi)\boldsymbol{e}_r \\ \boldsymbol{k}_2 = -\cos(\phi)\boldsymbol{e}_L + \sin(\phi)\boldsymbol{e}_r \end{cases} \tag{16}$$

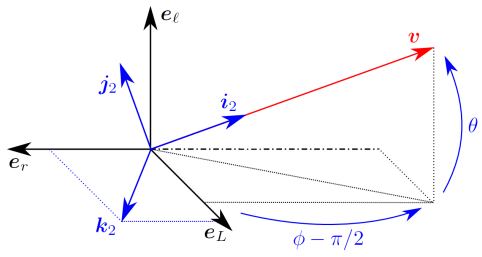

Fig. 2. Frame $(\boldsymbol{i}_2, \boldsymbol{j}_2, \boldsymbol{k}_2)$.

and the transformation from the frame $(\boldsymbol{e}_L, \boldsymbol{e}_\ell, \boldsymbol{e}_r)$ to the frame $(\boldsymbol{i}_2, \boldsymbol{j}_2, \boldsymbol{k}_2)$ is

$$R_b(\theta,\phi) = \begin{pmatrix} \cos(\theta)\sin(\phi) & \sin(\theta) & \cos(\theta)\cos(\phi) \\ -\sin(\theta)\sin(\phi) & \cos(\theta) & -\sin(\theta)\cos(\phi) \\ -\cos(\phi) & 0 & \sin(\phi) \end{pmatrix} \in SO(3)$$

The new local chart is $(U_b = \varphi_b^{-1}(U), \varphi_b)$ with

$$\varphi_b^{-1}(r,L,\ell,v,\theta,\phi) = \Big(r\cos(L)\cos(\ell), r\cos(L)\sin(\ell), \\ r\sin(L), R^T(L,\ell)\cdot R_b^T(\theta,\phi)\begin{pmatrix} v \\ 0 \\ 0 \end{pmatrix} \Big)$$

This local map covers the singularities w.r.t. the path angle γ of the chart (U_a, φ_a). In these new coordinates, the derivative of the velocity is

$$\begin{aligned} \dot{\boldsymbol{v}} &= \dot{v}\boldsymbol{i}_2 + \Big[v\dot{\theta} - \frac{v^2}{r}\sin(\theta)\big(\cos(\phi)+\sin(\phi)\tan(L)\big)\Big]\boldsymbol{j}_2 \\ &+ \Big[\frac{v^2}{r}\cos^2(\theta)\Big(\sin(\phi)+\tan^2(\theta)\Big(\sin(\phi)-\tan(L)\cos(\phi)\Big)\Big) \\ &- v\dot{\phi}\cos(\theta)\Big]\boldsymbol{k}_2 \end{aligned} \tag{17}$$

As previously, we now introduce new control variables (which are complementary to the local control $\boldsymbol{w}$), defining $\boldsymbol{z} = R_b(\theta,\phi)\cdot R(L,\ell)\boldsymbol{u}$. The constraints c_1 and c_2 are given in this local chart by

$$c_1(\boldsymbol{z}) = -z_1 \quad , \quad c_2(\boldsymbol{z}) = \frac{z_2^2+z_3^2}{\sin^2(\alpha_{\max})} - 1 \quad , \quad \boldsymbol{z}\in S^2 \tag{18}$$

Using the same notations as in the previous section, with the help of (17),the local evaluation of the dynamics of (1) using the chart φ_b gives

$$\begin{cases} \dot{r} = -v\cos(\theta)\cos(\phi)\ , \qquad \dot{L} = \dfrac{v}{r}\cos(\theta)\sin(\phi)\ , \qquad \dot{\ell} = \dfrac{v}{r}\dfrac{\sin(\theta)}{\cos(L)} \\ \dot{v} = \dfrac{f_T}{m}z_1 - \big(d+\eta c_m(z_2^2+z_3^2)\big)\,v^2 + g\cos(\theta)\cos(\phi) \\ \dot{\theta} = \omega z_2 + \dfrac{v}{r}\sin(\theta)\Big(\cos(\phi)+\sin(\phi)\tan(L)\Big) - \dfrac{g}{v}\sin(\theta)\cos(\phi) \\ \dot{\phi} = -\dfrac{\omega}{\cos(\theta)}z_3 + \dfrac{v}{r}\cos(\theta)\Big(\sin(\phi)+\tan^2(\theta)\Big(\sin(\phi) \\ \qquad -\tan(L)\cos(\phi)\Big)\Big) - \dfrac{g}{v}\dfrac{\sin(\phi)}{\cos(\theta)} \end{cases} \tag{19}$$

We define a new control problem, named (**GOGP**)$_b$, which consists in minimizing the cost function

$$C_T^b(r, L, \ell, v, \theta, \phi, \boldsymbol{z}) = g(T, \varphi_b^{-1}(r, L, \ell, v, \theta, \phi)(T))$$

subject to the dynamics (19) and to the control constraints (18). As (**GOGP**)$_a$, this is a classical pure control constraint optimal control problem that is locally equivalent to (**GOGP**).

Remark 2: The mappings $\varphi_a^{-1} : U \to \mathbb{R} \setminus \{0\}$, $\varphi_b^{-1} : U \to \mathbb{R} \setminus \{0\}$ are not defined respectively for the values $\chi = \pi$, $\phi = \pi$: these singularities can be covered by extending φ_a^{-1} and φ_b^{-1} also within $\tilde{U} = \left[(0, \infty) \times \left(-\frac{\pi}{2}, \frac{\pi}{2}\right) \times (0, 2\pi)\right]^2$. Moreover, the framework of this paper concerns launch vehicles able to cover bounded distances (in the region of one hundred kilometers). From these remarks, without loss of generality, we define the configuration manifold of (**GOGP**) as $N = U_a \cup U_b$.

C. Equivalence between Global and Local Maximum Principle Formulations

From the previous arguments, it is clear that, within $U_a \subseteq \mathbb{R}^6 \setminus \{0\}$, (**GOGP**) is equivalent to (**GOGP**)$_a$ while, within $U_b \subseteq \mathbb{R}^6 \setminus \{0\}$, (**GOGP**) is equivalent to (**GOGP**)$_b$. However, it is not clear that the Maximum Principle formulation related to (**GOGP**), which is a mixed control-state constraint problem, coincides respectively with the dual formulation of (**GOGP**)$_a$, locally within U_a, and with the dual formulation of (**GOGP**)$_b$, locally within U_b, which are pure control constraint problems. Indeed, we have a priori three different adjoint formulations, namely: $(\boldsymbol{p}(\cdot), p^0, \mu_1(\cdot), \mu_2(\cdot))$ related to (**GOGP**) and two multipliers $(p_a(\cdot), p_a^0)$ and $(p_b(\cdot), p_b^0)$ of the classical pure control constraint Maximum Principle formulations respectively related to (**GOGP**)$_a$ and (**GOGP**)$_b$. We shall prove that it is always possible, in these three applications of the PMP, to choose the multipliers so that the local projections of $(\boldsymbol{p}(\cdot), p^0)$ onto charts (U_a, φ_a) and (U_b, φ_b) coincide respectively with $(p_a(\cdot), p_a^0)$ and $(p_b(\cdot), p_b^0)$. More precisely, the following result holds.

Theorem 1: Consider the manifold $N = U_a \cup U_b \subseteq \mathbb{R}^6 \setminus \{0\}$ of all possible scenarios of (**GOGP**). Suppose that $(\boldsymbol{r}(\cdot), \boldsymbol{v}(\cdot), \boldsymbol{u}(\cdot))$ is an optimal solution of (**GOGP**) in $[0, T]$. There exist a multiplier $(\boldsymbol{p}(\cdot), p^0, \mu_1(\cdot), \mu_2(\cdot))$ satisfying the Maximum Principle formulation (4)-(9) and two multipliers $(p_a(\cdot), p_a^0)$, $(p_b(\cdot), p_b^0)$ related to the classical pure control constraint Maximum

Principle formulations respectively of (**GOGP**)$_a$ and (**GOGP**)$_b$, such that $p_a^0 = p_b^0 = p^0$ and

$$\boldsymbol{p}(t) = \begin{cases} (\varphi_a)^*_{\varphi_a(\boldsymbol{r}(t),\boldsymbol{v}(t))} \cdot p_a(t) \quad , \quad (\boldsymbol{r}(t),\boldsymbol{v}(t)) \in U_a \\ (\varphi_b)^*_{\varphi_b(\boldsymbol{r}(t),\boldsymbol{v}(t))} \cdot p_b(t) \quad , \quad (\boldsymbol{r}(t),\boldsymbol{v}(t)) \in U_b \end{cases} \tag{20}$$

where $(\cdot)^*$ denotes the pull-back operator.

The proof of Theorem 1 is reported in Appendix A. The main idea is the following. From the mixed constraint Maximum Principle, we recover a global adjoint vector $\boldsymbol{p}(\cdot)$ of (**GOGP**) and we localize it onto one of the two local charts built previously, for example, (U_a, φ_a). Then, exploiting the local maximality condition (6) and the previous transformation between $\boldsymbol{u}$ and $\boldsymbol{z}$, one shows that the covector $(\varphi_a)^* \cdot \boldsymbol{p}(\cdot)$ satisfies the classical pure control constraint Maximum Principle formulation related to (**GOGP**)$_a$.

Let us clarify how one could take advantage of this result to solve (**GOGP**) numerically by indirect methods. Assume to have an optimal solution $(\boldsymbol{r}(\cdot),\ \boldsymbol{v}(\cdot),\ \boldsymbol{u}(\cdot))$ of (**GOGP**), within $[0, T]$. Without loss of generality we can suppose that $(\boldsymbol{r}, \boldsymbol{v})(0) \in U_a$. If the optimal value of $\boldsymbol{p}(0)$ is known, from $p_a(0) = (\varphi_a^{-1})^*_{(\boldsymbol{r}(0),\boldsymbol{v}(0))}\boldsymbol{p}(0)$, we start a shooting method on (**GOGP**)$_a$. Suppose that, at a given time $\tau_1 \in (0, T)$, the optimal trajectory is such that $(\boldsymbol{r}, \boldsymbol{v})(\tau_1) \in U_b \setminus U_a$, i.e. our solution crosses a *singular region* of the first local chart. Then, we can stop momentarily the numerical computations at a time $\tau_2 < \tau_1$ such that $(\boldsymbol{r}, \boldsymbol{v})(\tau_2) \in U_a \cap U_b$ and starting from $p_b(\tau_2) = (\varphi_a \circ \varphi_b^{-1})^*_{\varphi_a(\boldsymbol{r}(\tau_2),\boldsymbol{v}(\tau_2))} p_a(\tau_2)$ a shooting method on (**GOGP**)$_b$, avoiding the geometrical singularity related to U_a when reaching the point $(\boldsymbol{r}, \boldsymbol{v})(\tau_1) \in U_b \setminus U_a$. This procedure can be iterated every time a jump from U_a to U_b (as well as a jump from U_b to U_a) occurs in the optimal trajectory. The adjoint vector related to (**GOGP**) is recovered thanks to (20). This methodology allows to describe optimal solutions of any feasible mission related to (**GOGP**).

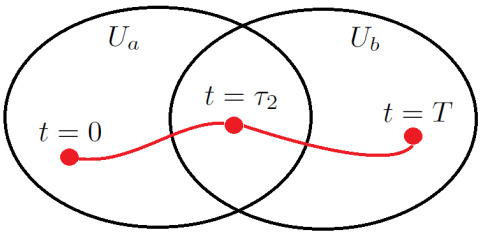

Fig. 3. Optimal trajectory crossing the domains of the two charts.

D. Optimal Control Synthesis

Let $(\boldsymbol{r}(\cdot), \boldsymbol{v}(\cdot), \boldsymbol{u}(\cdot))$ be an optimal solution of (**GOGP**) in $[0, T]$ and $\boldsymbol{p}(\cdot)$, $\boldsymbol{p}_a(\cdot) = (p_r^a, p_L^a, p_\ell^a, p_v^a, p_\gamma, p_\chi)(\cdot)$ and $\boldsymbol{p}_b(\cdot) = (p_r^b, p_L^b, p_\ell^b, p_v^b, p_\theta, p_\phi)(\cdot)$ be the adjoint vectors respectively of (**GOGP**), (**GOGP**)$_a$ and (**GOGP**)$_b$ as in Theorem 1. The computation of the optimal control $\boldsymbol{u}$ can be achieved by focusing on the optimal values of the local controls $\boldsymbol{w}$ and $\boldsymbol{z}$. Hereafter, when clear from the context, we skip the dependence on t to keep better readability. Denoting $C_a := p_v^a \frac{f_T}{m}$, $C_b := p_v^b \frac{f_T}{m}$, $D_a := p_v^a \eta c_m v^2$ and $D_b := p_v^b \eta c_m v^2$, from the pure control constraint Maximum Principle, locally almost everywhere where they are defined, the maximization conditions (5) related to (**GOGP**)$_a$ and (**GOGP**)$_b$ give respectively

$$\boldsymbol{w}(t) = \text{argmax}\Bigg\{ C_a w_1 - D_a(w_2^2 + w_3^2) + p_\gamma \omega w_2 + p_\chi \frac{\omega}{\cos(\gamma)} w_3 \;\; | \;\; w_1^2 + w_2^2 + w_3^2 = 1 \;,\; w_1 \geq 0 \;,\; w_2^2 + w_3^2 \leq \sin^2(\alpha_{\max}) \Bigg\} \tag{21}$$

$$\boldsymbol{z}(t) = \text{argmax}\Bigg\{ C_b z_1 - D_b(z_2^2 + z_3^2) + p_\theta \omega z_2 - p_\phi \frac{\omega}{\cos(\theta)} z_3 \;\; | \;\; z_1^2 + z_2^2 + z_3^2 = 1 \;,\; z_1 \geq 0 \;,\; z_2^2 + z_3^2 \leq \sin^2(\alpha_{\max}) \Bigg\} \,. \tag{22}$$

Solving these maximization conditions may lead to either *regular* or *singular controls*, depending on the value of the two couples $(p_\gamma(\cdot), p_\chi(\cdot))$ and $(p_\theta(\cdot), p_\phi(\cdot))$ respectively on non-zero mesure subsets.

By definition, regular controls are the regular points of the end-point mapping while singular controls are critical points of the end-point mapping. Then, with respect to (**GOGP**), regular controls consist of controls whose extremal, within a non-zero measure set $J \subseteq [0, T]$, satisfies either $p_\gamma|_J(\cdot) \neq 0 \;\vee\; p_\chi|_J(\cdot) \neq 0$ if the system travels along the first chart (U_a, φ_a) within J or $p_\theta|_J(\cdot) \neq 0 \;\vee\; p_\phi|_J(\cdot) \neq 0$ if the system covers the second chart (U_b, φ_b) within J and, conversely, singular controls consist of controls for which there exists a non-zero measure set $J \subseteq [0, T]$ such that $p_\gamma|_J(\cdot) = p_\chi|_J(\cdot) = 0$ in the first local chart, as well as $p_\theta|_J(\cdot) = p_\phi|_J(\cdot) = 0$ in the second chart.

1) Regular Controls: Suppose that, locally within a non-zero measure subset $J \subseteq [0, T]$, either $p_\gamma|_J(\cdot) \neq 0 \;\vee\; p_\chi|_J(\cdot) \neq 0$ if the system travels along the first chart (U_a, φ_a) within J or $p_\theta|_J(\cdot) \neq 0 \;\vee\; p_\phi|_J(\cdot) \neq 0$ if the system covers the second chart (U_b, φ_b) within J. In this case, regular controls appear.

Analytical expressions of these controls are derived from (21) and (22), by using Karush-Kuhn-Tucker conditions, under the following assumption:

Assumption 2: For points $(\varepsilon, x) \in \mathbb{R}_+ \times \mathbb{R}$ such that $(1+\varepsilon)x^2 \leq \sin^2(\alpha_{\max})$, where $0 < \alpha_{\max} \leq \pi/6$ is constant, the following second order Taylor approximation is considered: $\sqrt{1-(1+\varepsilon)x^2} \cong \Big(1-(1+\varepsilon)x^2/2\Big)$.

This assumption is not limiting because, for most of the launch vehicle applications considered using the dynamical model of (**GOGP**), the maximal angle of attack $\alpha_{\max}$ is actually lower than $\pi/6$. Moreover, this assumption has already implicitly been used to recover the analytical expressions of the drag and the lift listed in Section II-A (see [34] for further details).

The computation of the analytical expressions of regular controls is done in Appendix B. It is interesting to note that regular controls are well defined in each of the two charts (U_a, φ_a), (U_b, φ_b) but their local expressions tends to singular values as the optimal trajectory gets close respectively to the boundary of U_a or U_b.

2) Singular Controls: In some cases, locally within a non-zero measure subset $J \subseteq [0, T]$, it could happen that $p_\gamma|_J(\cdot) = p_\chi|_J(\cdot) = 0$ in the first local chart, as well as $p_\theta|_J(\cdot) = p_\phi|_J(\cdot) = 0$ in the second local chart. The control is then singular and the evaluation of an explicit analytical optimal strategy is harder to achieve than in the regular case. In this situation, (21) and (22) reduce to

$$\boldsymbol{w}(t) = \text{argmax}\Big\{C_a w_1 - D_a(w_2^2+w_3^2) \;\mid\; w_1^2+w_2^2+w_3^2 = 1, \quad w_1 \geq 0, w_2^2+w_3^2 \leq \sin^2(\alpha_{\max})\Big\} \tag{23}$$

$$\boldsymbol{z}(t) = \text{argmax}\Big\{C_b z_1 - D_b(z_2^2+z_3^2) \;\mid\; z_1^2+z_2^2+z_3^2 = 1, \quad z_1 \geq 0 \;,\; z_2^2+z_3^2 \leq \sin^2(\alpha_{\max})\Big\} \tag{24}$$

The Karush-Kuhn-Tucker conditions do not help anymore because, depending on the value of C_a or C_b, many uncountable values of (w_2, w_3) or (z_2, z_3) are optimal. Instead, a geometric study is required.

It is in the case of singular controls that Assumption 1 becomes particularly useful to manage hard computations, as well as the following one:

Assumption 3: Suppose that $J \subseteq [0,T]$ is of positive measure. Any optimal trajectory associated with a singular control in J satisfies, along J,

$$\text{if } f_T > 0 \ , \ \text{then } \|\boldsymbol{v}\| > \sqrt{\frac{3}{2} g(\boldsymbol{r}) h_r} \sqrt{\sqrt{1 + \frac{4}{9} \frac{1}{g(\boldsymbol{r}) h_r} \left(\frac{f_T}{md} \right)} - 1} \quad .$$

It is important to note that, for our applications, the magnitude of the velocities of the vehicles is large enough when $f_T > 0$, so that Assumption 3 is always satisfied, as numerical simulations confirm. In particular, it must be noticed that this assumption is required only for singular arcs i.e., if only regular optimal controls arise then no boundaries on the velocities are imposed.

Running several numerical Monte-Carlo simulations, we have not encoutered any singular arcs. However, for sake of completness, in this paper we provide the expressions of singular optimal controls in Appendix C, which lead straightforwardly to the proof of the following result.

Proposition 1: Under Assumption 1 and Assumption 3, any singular optimal control of (**GOGP**) is well-defined and has a univocal analytical expression.

IV. Numerical Resolution of (**GOGP**) via Homotopy Methods

A. Problem of Order Zero

To apply homotopy methods, a problem of order zero, from which the iterative shooting path starts, must be provided first. This problem should be, on one hand, handy to solve via basic shooting methods and, on the other hand, as close as possible to (**GOGP**) to recover easily the original solution.

The problem of order zero, denoted $(\mathbf{GOGP})_0$, consists in minimizing

$$C_T^0(\boldsymbol{r}(\cdot), \boldsymbol{v}(\cdot), \boldsymbol{u}(\cdot)) = g_0(T, \boldsymbol{r}(T), \boldsymbol{v}(T)) \tag{25}$$

subject to the simplified dynamics

$$\begin{cases} \dot{\boldsymbol{r}}(t) = \boldsymbol{v}(t) \quad , \quad \dot{\boldsymbol{v}}(t) = \boldsymbol{f}_0(t, \boldsymbol{r}(t), \boldsymbol{v}(t), \boldsymbol{u}(t)) \\ (\boldsymbol{r}(t), \boldsymbol{v}(t)) \in N \quad , \quad \boldsymbol{u}(t) \in S^2 \quad , \quad (\boldsymbol{r}(T), \boldsymbol{v}(T)) \in M_0 \subseteq N \\ c_1(\boldsymbol{v}(t), \boldsymbol{u}(t)) := -\boldsymbol{v}(t) \cdot \boldsymbol{u}(t) \leq 0 \quad , \quad \boldsymbol{r}(0) = \boldsymbol{r}_0 \ , \ \boldsymbol{v}(0) = \boldsymbol{v}_0 \\ c_2(\boldsymbol{v}(t), \boldsymbol{u}(t)) := \left(\frac{\|\boldsymbol{u}(t) \wedge \boldsymbol{v}(t)\|}{\|\boldsymbol{v}(t)\| \sin \alpha_{\max}} \right)^2 - 1 \leq 0 \end{cases}$$

Here, the user can choose the cost $g_0(T, \boldsymbol{r}(T), \boldsymbol{v}(T))$, the dynamics $\boldsymbol{f}_0(t, \boldsymbol{r}, \boldsymbol{v}, \boldsymbol{u})$ and the target submanifold M_0. Dynamics $\boldsymbol{f}_0(t, \boldsymbol{r}, \boldsymbol{v}, \boldsymbol{u})$ is chosen to remove bothersome contributions, that is

$$\boldsymbol{f}_0(t, \boldsymbol{r}, \boldsymbol{v}, \boldsymbol{u}) = \boldsymbol{f}(t, \boldsymbol{r}, \boldsymbol{v}, \boldsymbol{u}) - \left(\boldsymbol{\omega}_{\text{NED}}(\boldsymbol{r}, \boldsymbol{v}) \wedge \boldsymbol{v} + \frac{\boldsymbol{T}(t, \boldsymbol{u})}{m} + \frac{\boldsymbol{g}(\boldsymbol{r})}{m} \right) \tag{26}$$

where $\boldsymbol{\omega}_{\text{NED}}(\boldsymbol{r}, \boldsymbol{v})$ represents the angular velocity of the NED frame $(\boldsymbol{e}_L, \boldsymbol{e}_l, \boldsymbol{e}_r)$ w.r.t. the inertial frame $(\boldsymbol{I}, \boldsymbol{J}, \boldsymbol{K})$ and it is important to evaluate (26) strictly onto charts (U_a, φ_a), (U_b, φ_b), otherwise its analytical expression could be more complex than the original dynamics. Moreover, M_0 is chosen such that non-challenging maneuvers suffice to reach the target with an optimal behavior.

The resolution of (**GOGP**)$_0$ by standard indirect methods leads to a simplified solution $(\boldsymbol{r}_0(\cdot), \boldsymbol{v}_0(\cdot), \boldsymbol{u}_0(\cdot))$ with extremal $(\boldsymbol{p}_0(\cdot), p_0^0)$. Led by the previous results, from now on, we avoid to report the multipliers related to the mixed contraints.

*B. Homotopy Method Starting from (**GOGP**)$_0$*

We first introduce the family of problems (**GOGP**)$_{\boldsymbol{\lambda}}$, depending on the parameter $\boldsymbol{\lambda}$. Each problem consists in minimizing the parametrized cost

$$C_T^{\boldsymbol{\lambda}}(\boldsymbol{r}(\cdot), \boldsymbol{v}(\cdot), \boldsymbol{u}(\cdot)) = g_{\boldsymbol{\lambda}}(T, \boldsymbol{r}(T), \boldsymbol{v}(T))$$

subject to the parametrized dynamics

$$\begin{cases} \dot{\boldsymbol{r}}(t) = \boldsymbol{v}(t) \quad , \quad \dot{\boldsymbol{v}}(t) = \boldsymbol{f}_{\boldsymbol{\lambda}}(t, \boldsymbol{r}(t), \boldsymbol{v}(t), \boldsymbol{u}(t)) \\ (\boldsymbol{r}(t), \boldsymbol{v}(t)) \in N \quad , \quad \boldsymbol{u}(t) \in S^2 \quad , \quad (\boldsymbol{r}(T), \boldsymbol{v}(T)) \in M_{\boldsymbol{\lambda}} \subseteq N \\ c_1(\boldsymbol{v}(t), \boldsymbol{u}(t)) := -\boldsymbol{v}(t) \cdot \boldsymbol{u}(t) \leq 0 \quad , \quad \boldsymbol{r}(0) = \boldsymbol{r}_0 \ , \ \boldsymbol{v}(0) = \boldsymbol{v}_0 \\ c_2(\boldsymbol{v}(t), \boldsymbol{u}(t)) := \left(\frac{\|\boldsymbol{u}(t) \wedge \boldsymbol{v}(t)\|}{\|\boldsymbol{v}(t)\| \sin \alpha_{\max}} \right)^2 - 1 \leq 0 \end{cases}$$

There are no restrictions on the choice of the parameter $\boldsymbol{\lambda}$, usually a vector of some metric space. It could be a physical parameter as well as an artificial variable. The family of problems is built such that, for $\boldsymbol{\lambda} = 0$, (**GOGP**)$_{\boldsymbol{\lambda}}$ is equivalent to (**GOGP**)$_0$, while, it exists some value $\hat{\boldsymbol{\lambda}}$, such that (**GOGP**)=(**GOGP**)$_{\hat{\boldsymbol{\lambda}}}$.

If one is able to solve (**GOGP**)$_{\boldsymbol{\lambda}}$, a solution $(\boldsymbol{r}_{\boldsymbol{\lambda}}(\cdot), \boldsymbol{v}_{\boldsymbol{\lambda}}(\cdot), \boldsymbol{u}_{\boldsymbol{\lambda}}(\cdot))$ with extremal $(\boldsymbol{p}_{\boldsymbol{\lambda}}(\cdot), p_{\boldsymbol{\lambda}}^0)$ is found. The aim of the homotopy procedure consists then in seeking the solution $(\boldsymbol{r}_{\hat{\boldsymbol{\lambda}}}(\cdot), \boldsymbol{v}_{\hat{\boldsymbol{\lambda}}}(\cdot), \boldsymbol{u}_{\hat{\boldsymbol{\lambda}}}(\cdot))$

with extremal $(\boldsymbol{p}_{\hat{\boldsymbol{\lambda}}}(\cdot), p^0_{\hat{\boldsymbol{\lambda}}})$ of the original problem $(\mathbf{GOGP})_{\hat{\boldsymbol{\lambda}}}$, starting from the solution $(\boldsymbol{r}_0(\cdot), \boldsymbol{v}_0(\cdot), \boldsymbol{u}_0(\cdot))$ with extremal $(\boldsymbol{p}_0(\cdot), p^0_0)$ of the problem of order zero, by making $\boldsymbol{\lambda}$ converge to $\hat{\boldsymbol{\lambda}}$.

An example of a parametrized family of problems $(\mathbf{GOGP})_{\boldsymbol{\lambda}}$ is given hereafter, exploiting the considerations of Section IV-A. We set $\boldsymbol{\lambda} = (\lambda_1, \lambda_2) \in [0,1]^2$ to be the homotopic parameter and we define

$$g_{\boldsymbol{\lambda}}(T, \boldsymbol{r}, \boldsymbol{v}) := g_0(T, \boldsymbol{r}, \boldsymbol{v}) + \lambda_1 \Big(g(T, \boldsymbol{r}, \boldsymbol{v}) - g_0(T, \boldsymbol{r}, \boldsymbol{v}) \Big) \tag{27}$$

$$\boldsymbol{f}_{\boldsymbol{\lambda}}(t, \boldsymbol{r}, \boldsymbol{v}, \boldsymbol{u}) := \boldsymbol{f}(t, \boldsymbol{r}, \boldsymbol{v}, \boldsymbol{u}) - (1-\lambda_1) \left(\boldsymbol{\omega}_{\text{NED}}(\boldsymbol{r}, \boldsymbol{v}) \wedge \boldsymbol{v} + \frac{\boldsymbol{T}(t, \boldsymbol{u})}{m} + \frac{\boldsymbol{g}(\boldsymbol{r})}{m} \right) \tag{28}$$

while λ_2 acts only on M_0 and it is such that $M \equiv M_{\lambda_2 = 1}$. We see that the original problem corresponds to $\boldsymbol{\lambda} = (1,1)$. The idea of splitting the homotopic parameter into two components (λ_1 and λ_2) helps to treat separately the hard terms of the dynamics and the mission involved (see Section V).

Note that homotopy methods may fail whenever, during the iteration path, bifurcation points, singularities or different connected components are encountered (we refer to [38], [1] for details). However, numerical simulations show that our choice of the problem of order zero $(\mathbf{GOGP})_0$ is such that the main structure of the solutions of the original problem (**GOGP**) is mantained, which makes the homotopy procedure converge correctly.

V. Launch Vehicle Application: Endo-Atmospheric Missile Interception

The context is the *endo-atmospheric interception*. The problem consists in steering a missile towards a (usually) fast target, minimizing some criterion. We are interested in the *mid-course phase* which starts when the vehicle reaches a given threshold of the magnitude of the velocity. The target consists of a predicted interception point. This point may change over time, and then, accurate computations are needed.

Our Optimal Interception Problem (**OIP**) consists in minimizing the cost

$$C_T(\boldsymbol{r}(\cdot), \boldsymbol{v}(\cdot), \boldsymbol{u}(\cdot)) = C_1 T - \|\boldsymbol{v}(T)\|^2 + C_2 \int_0^T \left(\frac{\|\boldsymbol{u}(t) \wedge \boldsymbol{v}(t)\|}{\|\boldsymbol{v}(t)\|} \right)^2 dt \tag{29}$$

where $0 \leq C_1 \leq 1$, $C_2 \geq 0$ are constant, under the smooth dynamical control system (2), with a free final time T. This cost is set up to maximize the chances to reach the target with reasonable delays. The final manifold M is

$$M = \left\{ (\boldsymbol{r}, \boldsymbol{v}) \in N \;\; | \;\; \boldsymbol{r} = \boldsymbol{r}_1 \;, \;\; \frac{\boldsymbol{v} \cdot \boldsymbol{e}_r}{\|\boldsymbol{v}\|} = \cos(\psi_1), \right. \tag{30}$$

$$\left.\frac{\boldsymbol{v}\cdot\boldsymbol{e}_L}{\|\boldsymbol{v}\|}=\cos(\psi_2)\ ,\ \frac{\boldsymbol{v}\cdot\boldsymbol{e}_l}{\|\boldsymbol{v}\|}=\sin(\psi_2)\right\}$$

where $\boldsymbol{r}_1$ is a fixed final position and ψ_1 and ψ_2 are fixed angles. In other words, the final position and the direction of the final velocity are fixed, letting the modulus of the final velocity free. This choice is coherent with cost (29) and the fact that better chances of complete the mission arise if specific orientations of the missile are ensured. One can note that Assumption 1 is satisfied.

We propose to solve (**OIP**) by homotopy, applying verbatim the procedure presented in Section IV. In particular, we proceed using (27) and (28) to define the family of parametrized problems (**OIP**)$_{\boldsymbol{\lambda}}$, where $\boldsymbol{\lambda}=(\lambda_1,\lambda_2)\in[0,1]^2$ and λ_2 acts on the final submanifold only (as explained in Section IV-B).

*A. Simplified Problem (**OIP**)$_0$*

We need to provide good candidates for the simplified cost (25) and the submanifold M_0, such that, the optimal solution of the problem of order zero (**OIP**)$_0$ will initialize successfully the homotopy procedure.

Without loss of generality, the problem of order zero can be chosen such that its optimal trajectory lies in the domain of the first chart. Following the procedure provided is Section IV-A, one shows that (**OIP**)$_0$ can be selected as

$$(\mathbf{OIP})_0\begin{cases}\min\quad -v^2(T)\quad,\quad (w_2,w_3)\in\mathbb{R}^2\\ \dot r=v\sin(\gamma)\ ,\ \dot L=\dfrac{v}{r}\cos(\gamma)\cos(\chi)\ ,\ \dot l=\dfrac{v}{r}\dfrac{\cos(\gamma)\sin(\chi)}{\cos(L)}\\ \dot v=-(d+\eta c_m(w_2^2+w_3^2))v^2\ ,\ \dot\gamma=vc_mw_2\ ,\ \dot\chi=\dfrac{vc_m}{\cos(\gamma)}w_3\end{cases}$$

where the contribution of the thrust and the gravity are removed, no boundaries on the controls are imposed and $C_1=C_2=0$. More specifically, by applying the Maximum Principle to (**OIP**)$_0$ under appropriate assumptions, one is able to recover an approximated analytical guidance law which actually initializes successfully the entire homotopy procedure to solve (**OIP**). For sake of conciseness, we do not report the details (the interested reader can find the whole treatise in [4]).

B. Numerical Simulations

For the numerical simulations, we use predictor-corrector (PC) continuation methods. More precisely, we make parameters λ_1, λ_2 converge to 1 by using a standard linear continuation, ensuring a fast convergence of the predictor-corrector method. Moreover, we first act on the contribution of the gravity/thrust (by λ_1), then we recover the original scenario (by λ_2). Note that the PC continuation method is discrete, in contrast with differential methods, for which the Jacobian of the homotopy method must be computed (for further details, see [1], [9]). The shooting method is solved using the C routines *hybrd.c* [16] while a fixed time-step explicit fourth-order Runge-Kutta method is used to integrate differential equations (whose number of integration steps varies between 250 and 350).

A *solid-fuel propelled missile* is simulated. Below, its numerical values:

- $c_m(0) = 0.00075$ m^{-1}, $d(0) = 0.00005$ m^{-1}, $\eta = 0.442$, $h_r = 7500$ m and $\alpha_{\max} = \pi/6$;
- $\dfrac{q}{m_0}(t) \;=\; \begin{cases} 0.025 \text{ s}^{-1} \ , \ t \leq 20 \\ 0 \ , \ t > 20 \end{cases} , \dfrac{f_T}{m_0}(t) \;=\; \begin{cases} 37.5 \text{ m} \cdot \text{s}^{-2} \ , \ t \leq 20 \\ 0 \ , \ t > 20 \end{cases}$
- We fix the modulus of the initial velocity: $v(0) = 500$ m/s.

We consider four tests. Without loss of generality, we choose two scenarios whose initial and final targets lie in the domain of the first local chart U_a, which we always represent by their local coordinates $(\boldsymbol{r}, \boldsymbol{v}) \cong (r, L, l, v, \gamma, \chi)$ (reported in standard units). For each scenario we investigate two different cost functions. The initial point $(\boldsymbol{r}_0, \boldsymbol{v}_0)$ is fixed to the value $(r_T + 1000, 0, 0, 500, 0, 0)$. Moreover, we fix also the solution of $(\mathbf{OIP})_0$ (from which the whole homotopy procedure starts) to the trajectory arising considering as simplified final target manifold the following set

$$M_0 = \Big\{ (r - r_T, L \cdot r_T, l \cdot r_T) = (5000, 14000, 0) \quad , \quad (\gamma, \chi) = (0, 0) \Big\} \ .$$

1) First Scenario: Simple Mission: We consider first a standard and accessible mission. The corresponding final target manifold (30) is

$$M = \Big\{ (r - r_T, L \cdot r_T, l \cdot r_T) = (5000, 14000, -2000), \\ (\gamma, \chi) = (-\pi/6, \pi/6) \Big\} \ .$$

The two tests arising from this scenario are given respectively by the following forms of cost function (29)

$$(\mathbf{OIP})^1 \ : \ C_T(v) = -v^2(T) \quad , \quad (\mathbf{OIP})^1_T \ : \ C_T(v) = T - v^2(T) \ .$$

Problem $(\mathbf{OIP})_T^1$ represents a more realistic variety of interception missions. Referring to the procedure detailed in Section IV, we note that parameter λ_1 acts only in the cost function of $(\mathbf{OIP})_T^1$.

Solving these two problems by means of homotopy methods gives respectively $(T, C_T(v))_{(\mathbf{OIP})^1} = (22.1, -(803.8)^2)$ and $(T, C_T(v))_{(\mathbf{OIP})_T^1} = (21.4,\ -(753.7)^2)$ as optimal values. The simulations take around 0.9 s for $(\mathbf{OIP})^1$, for which 7 iterations on λ_1 and 9 on λ_2 are required, and 1.5 s for $(\mathbf{OIP})_T^1$, where rather 17 iterations on λ_1 and 15 on λ_2 are required. The gap in the number of iterations needed is explained by the presence of the minimal time in $(\mathbf{OIP})_T^1$ which makes the structure of the solutions more complicated.

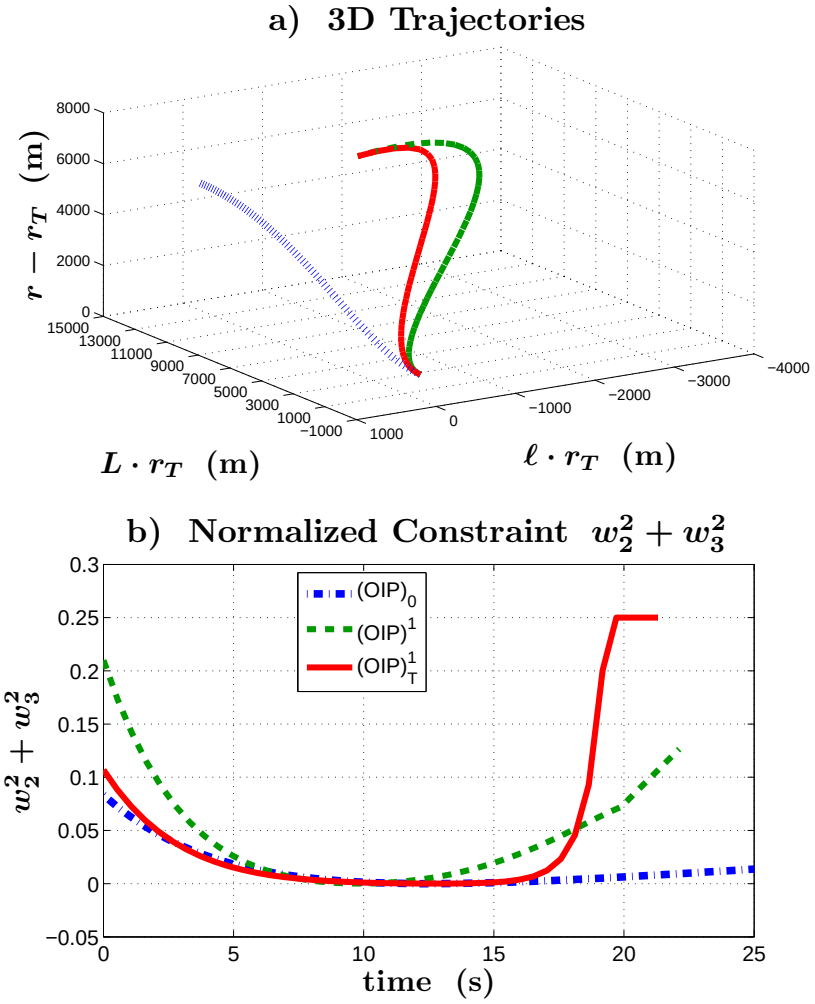

Fig. 4. Optimal solutions of problems $(\mathbf{OIP})^1$ and $(\mathbf{OIP})_T^1$.

Figure 4 shows the optimal solutions of this test case. The blue dot-dashed line represents the solution of $(\mathbf{OIP})_0$ which is obtained in around 0.15 s. Figure 4 b) shows $w_2^2(\cdot) + w_3^2(\cdot)$ which saturates at the value 0.25. From this picture, it is interesting to notice that, again, the minimal time obliges the controller to take abrupter maneuvers and then bang arcs arise more naturally.

2) Second Scenario: Complex Mission: The second mission considered is more challenging. Proposing to intercept a target quite close to the initial point, the vehicle is led to perform abrupt maneuvers to recover an optimal solution.

The final target manifold (30) is

$$M = \Big\{ (r - r_T, L \cdot r_T, l \cdot r_T) = (9000, 7500, 2000), \\ (\gamma, \chi) = (-\pi/4, -\pi/4) \Big\} \ .$$

The same cost functions as before are taken, i.e. with respect to the previous notations we consider the two problems $(\mathbf{OIP})^2$ and $(\mathbf{OIP})_T^2$.

The optimal values are respectively $(T, C_T(v))_{(\mathbf{OIP})^2} = (33.56, -(437.6)^2)$ and $(T, C_T(v))_{(\mathbf{OIP})_T^2} = (33.5, -(401.4)^2)$, and simulations take around 2.2 s for $(\mathbf{OIP})^2$ (7 iterations on λ_1 and 21 on λ_2), and 5.5 s for $(\mathbf{OIP})_T^1$ (17 iterations on λ_1 and 78 on λ_2). In this test, the difference between the trajectories related to $(\mathbf{OIP})^2$ and $(\mathbf{OIP})_T^2$ is quite imperceptible. This is understood by inspecting the normalized constraint in Figure 5 b). The two optimal strategies saturate most of the time and almost at the same point, because of the abrupt maneuvers needed to reach the target.

More interestingly, a change of local chart (from (U_a, φ_a) to (U_b, φ_b)) occurs. Indeed, the optimal trajectory is close twice to the critical value $\gamma = \pi/2$. In this case, the change of coordinates is not compulsory but it increases considerably the performances of the algorithm. Indeed, without it, simulations take 4 s for $(\mathbf{OIP})^2$ and 23 s for $(\mathbf{OIP})_T^2$. Anyhow, other tests show that some scenarios cannot be solved without the change of local chart.

All the four tests were treated also with a non-initialized direct method (AMPL combined with IPOPT, using 200 time steps, see [17]). Modifying the initial guess of IPOPT, these problems are solved by the direct method with computational times at least comparable to the ones given by our method, obtaining the good optimal solutions but less accurately. Moreover, when $(\mathbf{OIP})^2$ and $(\mathbf{OIP})_T^2$ are considered, the computational time of the direct method increases fast because of the presence of singularities. The modified indirect approach reveals itself to be very efficient, and sometimes, more successful than direct methods.

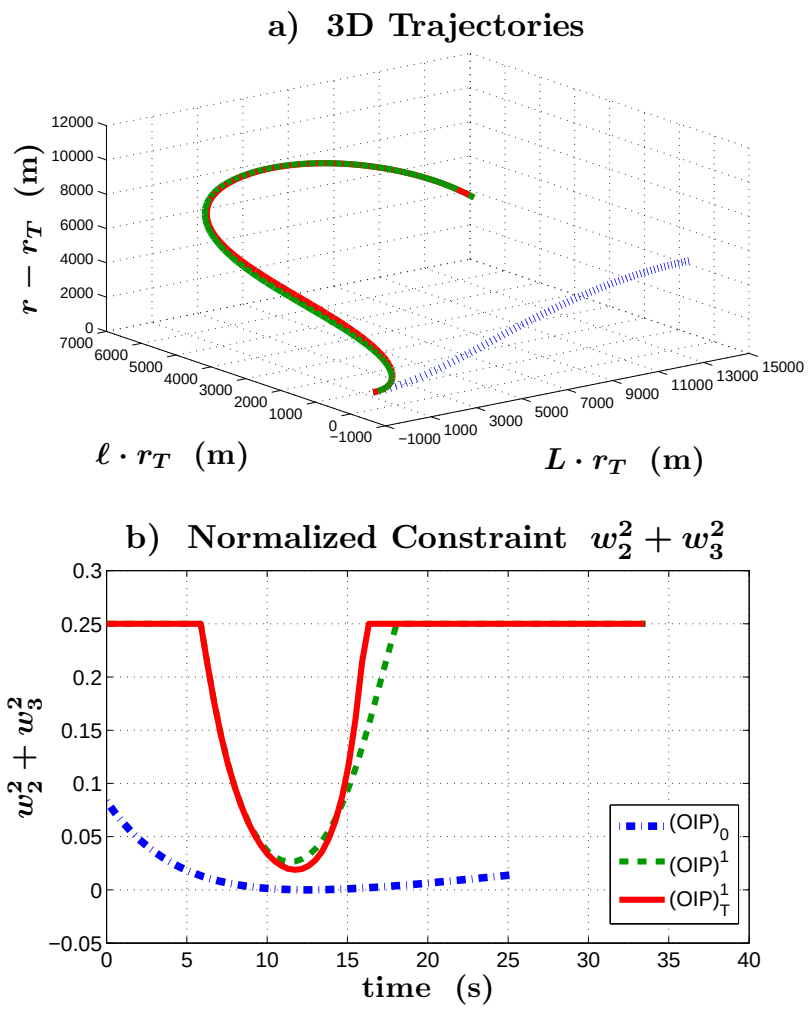

Fig. 5. Optimal quantities of problems (**OIP**)^2 and (**OIP**)^2_T.

VI. Conclusions and Perspectives

In this paper we have proposed a theoretical analysis and a numerical procedure to solve optimal control problems for endo-atmospheric launch vehicle systems.

Expressing the problem in an intrinsic geometric way, we have solved it by restricting to two local representations (in the sense of local charts in differential geometry on manifolds). The change of local chart that we have used appears to be instrumental in order to make numerical methods converge when the optimal strategy meets or is close to Euler singularities. We have exploited these local behaviors to provide the whole structure of optimal controls, as functions

of the state and the costate. Moreover, we have proved that every singular arc has a particular analytical form.

Our numerical procedure combines indirect methods with homotopy methods. Using this scheme, we have addressed the problem of a missile interception. We have solved the optimal control problem by acting on two parameters of deformation: the first one recovers the contribution of the thrust and the gravity, previously removed in the problem of order zero, while the second parameter leads to the final scenario. Numerical simulations on endo-atmospheric interception scenarios show the efficiency of our approach.

Future works will focus on the improvement of the dynamical model and of the computational times.

The dynamical model can be improved by considering the *non-minimum phase* phenomenon, a classical issue for launch vehicles applications (see, e.g. [3]), which can be modelled by delays. Motivated by the convergence result established in [5], the idea consists in adding the delay to the model by continuation.

For the computational time, even if many simulations on different scenarios show that the computation of optimal trajectories by using our approach takes on average 0.5-1 Hz, we cannot ensure a real-time processing yet. However, this is achieved by applying the continuation algorithm offline first. Indeed, we can evaluate offline optimal strategies for several possible scenarios, and then, and recover online, by spatial continuation (i.e. on the continuation parameter λ_2), the solution of a new mission with few homotopic iterations, which takes only milliseconds.

APPENDIX

A. *Proof of Theorem 1*

Here, we provide a proof of Theorem 1. In the following, we interpret the set of all possible scenarios $N = U_a \cup U_b$ as a manifold of dimension 6. Moreover, the constraint c_1 is never active and S^2 represents a constraint which is parametrizable in $\mathbb{R}^2$. Then, we remove these constraints from the formulation without loss of generality, supposing to seek an optimal control $\boldsymbol{u}(\cdot)$ of (**GOGP**) in $\mathbb{R}^3$ satisfying c_2 with a fixed final time T.

By similarity between the charts (U_a, φ_a) and (U_b, φ_b), we prove the assert only for the first chart (U_a, φ_a).

Let $(\boldsymbol{q}(\cdot), \boldsymbol{u}(\cdot))$ be an optimal solution of (**GOGP**) in $[0,T]$, where we denote $\boldsymbol{q} = (\boldsymbol{r}, \boldsymbol{v})$. Select $s_1, s_2 \in (0,T)$ such that $s_1 < s_2$, $\boldsymbol{q}([s_1,s_2]) \subseteq U_a$ and denote $x_a(\cdot) = \varphi_a^{-1} \circ \boldsymbol{q}(\cdot)$. Problem (**GOGP**) is written as

$$(\textbf{GOGP}) \quad \begin{cases} \min \quad \displaystyle\int_0^T f^0\big(t, \boldsymbol{q}_{\boldsymbol{\nu}}(t), \boldsymbol{\nu}(t)\big)\, dt \\ \dot{\boldsymbol{q}}_{\boldsymbol{\nu}}(t) = \boldsymbol{h}\big(t, \boldsymbol{q}_{\boldsymbol{\nu}}(t), \boldsymbol{\nu}(t)\big), \\ \boldsymbol{q}_{\boldsymbol{\nu}}(0) = \boldsymbol{q}_0 \ , \ \boldsymbol{q}_{\boldsymbol{\nu}}(T) \in M \\ c_2\big(\boldsymbol{q}_{\boldsymbol{\nu}}(t), \boldsymbol{\nu}(t)\big) \leq 0 \ , \ \text{a.e. } [0,T] \end{cases}$$

where f^0 is the Lagrange form of the Mayer cost of (**GOGP**), while, recalling the notations of Section III-B, its local version in the chart (U_a, φ_a) writes as

$$(\textbf{GOGP})_a \begin{cases} \min \ \displaystyle\int_{s_1}^{s_2} f^0\big(t, \varphi_a^{-1} \circ y_a(t), \Phi\big(y_a(t), \boldsymbol{\nu}'(t)\big)\big)\, dt \\ \dot{y}_a(t) = d(\varphi_a) \cdot \boldsymbol{h}\big(t, \varphi_a^{-1} \circ y_a(t), \Phi\big(y_a(t), \boldsymbol{\nu}'(t)\big)\big) \\ y_a(0) = \varphi_a^{-1}(\boldsymbol{q}_0) \ , \ y_a(s) = \varphi_a^{-1}(\boldsymbol{q}(s)) \\ c_2\big(\varphi_a^{-1} \circ y_a(t), \Phi\big(y_a(t), \boldsymbol{\nu}'(t)\big)\big) \leq 0 \ , \ \text{a.e. } [s_1, s_2] \\ \boldsymbol{\nu}'(\cdot) \in \mathcal{V}_a \end{cases}$$

where

$$\Phi : U \times \mathbb{R}^3 \to \mathbb{R}^3 : (x, \boldsymbol{\nu}') \mapsto R^\top(x) \cdot R_a^\top(x) \boldsymbol{\nu}'$$

is smooth and $\mathcal{V}_a$ is an open neighborhood of $\boldsymbol{z}(\cdot) = R_a(x_a(\cdot)) \cdot R(x_a(\cdot)) \boldsymbol{u}|_{[s_1,s_2]}(\cdot)$ in $L^\infty([s_1,s_2], \mathbb{R}^3)$ such that every trajectory of the vector field $d(\varphi_a) \cdot \boldsymbol{h}\big(t, \varphi_a^{-1}(x), \Phi(x, \boldsymbol{\nu}')\big)$ is contained in U for every $\boldsymbol{\nu}'(\cdot) \in \mathcal{V}_a$. The introduction of $\mathcal{V}_a$ is not limiting since the study of necessary conditions is local. An optimal solution of (**GOGP**)$_a$ is then $(x_a(\cdot), \boldsymbol{z}(\cdot))$.

Applying the Maximum Principle to (**GOGP**), we obtain a non-positive scalar p^0, an absolutely continuous mapping $\boldsymbol{p} : [0,T] \to T^*N \simeq \mathbb{R}^6$ and a function $\mu(\cdot) \in L^\infty([0,T], \mathbb{R})$, with $(\boldsymbol{p}(\cdot), p^0) \neq 0$, such that, denoting

$$H^0(t, \boldsymbol{q}, \boldsymbol{p}, p^0, \boldsymbol{u}) = \boldsymbol{p} \cdot \boldsymbol{h}(t, \boldsymbol{q}, \boldsymbol{u}) + p^0 f^0(t, \boldsymbol{q}, \boldsymbol{u}) \ ,$$

almost everywhere in $[0,T]$, there hold

$$\dot{\boldsymbol{p}}(t) = -\frac{\partial H^0}{\partial \boldsymbol{q}}(t,\boldsymbol{q}(t),\boldsymbol{p}(t),p^0,\boldsymbol{u}(t)) - \mu(t)\cdot\frac{\partial c_2}{\partial \boldsymbol{q}}(\boldsymbol{q}(t),\boldsymbol{u}(t)) \tag{31}$$

$$H^0(t,\boldsymbol{q}(t),\boldsymbol{p}(t),p^0,\boldsymbol{u}(t)) \geq H^0(t,\boldsymbol{q}(t),\boldsymbol{p}(t),p^0,\boldsymbol{u}) \tag{32}$$

$$\text{for every } \boldsymbol{u} \text{ such that} \quad c_2(\boldsymbol{q}(t),\boldsymbol{u}) \leq 0$$

$$\frac{\partial H^0}{\partial \boldsymbol{u}}(t,\boldsymbol{r}(t),\boldsymbol{v}(t),\boldsymbol{p}(t),p^0,\boldsymbol{u}(t)) + \mu(t)\cdot\frac{\partial c_2}{\partial \boldsymbol{u}}(\boldsymbol{q}(t),\boldsymbol{u}(t)) = 0 \tag{33}$$

and, furthermore, conditions (7)-(9) hold.

Since the quantity $c_2\big(\boldsymbol{q},\Phi\big(\varphi_a(\boldsymbol{q}),\boldsymbol{\nu}'\big)\big)$ does not depend on the state $\boldsymbol{q}$, deriving it w.r.t. $\boldsymbol{q}$ at $(\boldsymbol{q}(t),\boldsymbol{z}(t))$, one obtains

$$\frac{\partial c_2}{\partial \boldsymbol{q}}(\boldsymbol{q}(t),\boldsymbol{u}(t)) + \frac{\partial c_2}{\partial \boldsymbol{u}}(\boldsymbol{q}(t),\boldsymbol{u}(t))\cdot\frac{\partial \Phi}{\partial \boldsymbol{q}}(x_a(t),\boldsymbol{z}(t)) = 0\ .$$

Multiplying the previous expression by $\mu(t)$ and plugging it into (33), we have that

$$\mu(t)\cdot\frac{\partial c_2}{\partial \boldsymbol{q}}(\boldsymbol{q}(t),\boldsymbol{u}(t)) = \frac{\partial H^0}{\partial \boldsymbol{u}}(t,\boldsymbol{r}(t),\boldsymbol{v}(t),\boldsymbol{p}(t),p^0,\boldsymbol{u}(t))\cdot\frac{\partial \Phi}{\partial \boldsymbol{q}}(x_a(t),\boldsymbol{z}(t))$$

such that, for almost every $t\in[s_1,s_2]$, the adjoint equation (31) becomes

$$\dot{\boldsymbol{p}}(t) = -\frac{\partial H^0}{\partial \boldsymbol{q}}(t,\boldsymbol{q}(t),\boldsymbol{p}(t),p^0,\boldsymbol{u}(t)) \tag{34}$$
$$-\frac{\partial H^0}{\partial \boldsymbol{u}}(t,\boldsymbol{r}(t),\boldsymbol{v}(t),\boldsymbol{p}(t),p^0,\boldsymbol{u}(t))\cdot\frac{\partial \Phi}{\partial \boldsymbol{q}}(x_a(t),\boldsymbol{z}(t))\ .$$

Then, by defining $p_a(t) = (\varphi_a^{-1})^*_{\boldsymbol{q}(t)}\cdot\boldsymbol{p}(t)$ for every $t\in[s_1,s_2]$, it is straightforward to obtain from (34) the following adjoint equation

$$\dot{p}_a(t) = -p_a(t)\cdot\frac{\partial[d(\varphi_a)\cdot\boldsymbol{h}\big(t,\varphi_a^{-1}(x),\Phi(x,\boldsymbol{\nu}')\big)]}{\partial x}(t,x_a(t),\boldsymbol{z}(t)) \tag{35}$$
$$-p^0\frac{\partial[f^0\big(t,\varphi_a^{-1}(x),\Phi(x,\boldsymbol{\nu}')\big)]}{\partial x}(t,x_a(t),\boldsymbol{z}(t)) \quad .$$

Moreover, from the properties of Φ, the maximality condition (32) reads also

$$H_a^0(t,x_a(t),p_a(t),p^0,\boldsymbol{z}(t)) \geq H_a^0(t,\boldsymbol{q}(t),\boldsymbol{p}(t),p^0,\boldsymbol{z}) \tag{36}$$

$$\text{for every } \boldsymbol{z} \text{ such that} \quad c_2\big(\varphi_a^{-1}\circ x_a(t),\Phi\big(x_a(t),\boldsymbol{z}\big)\big) \leq 0$$

where

$$H_a^0(t,x,p,p^0,\boldsymbol{z}) = p\cdot d(\varphi_a)\cdot\boldsymbol{h}\big(t,\varphi_a^{-1}(x),\Phi(x,\boldsymbol{z})\big)$$

$$+p^0 f^0\big(t, \varphi_a^{-1}(x), \Phi(x, \boldsymbol{z})\big)$$

From conditions (35) and (36), we deduce that $(p_a(\cdot), p^0)$ is the sought multiplier for the Maximum Principle formulation of (**GOGP**)$_a$. The conclusion follows.

B. Computation of Regular Controls

In this section we compute regular optimal controls for (**GOGP**), under Assumption 2. We start supposing that the system is described by using the first local chart (U_a, φ_a) in a non-zero mesure subset $J \subseteq [0, T]$. Then, $p_\gamma|_J(\cdot) \neq 0$ or $p_\chi|_J(\cdot) \neq 0$.

If $p_v^a|_J(\cdot) = 0$, by definition $C_a|_J(\cdot) = D_a|_J(\cdot) = 0$ and then, from (21) and the Cauchy-Schwarz inequality, we obtain

$$w_2 = \frac{\sin(\alpha_{\max}) p_\gamma}{\sqrt{p_\gamma^2 + \frac{p_\chi^2}{\cos^2(\gamma)}}} \quad , \quad w_3 = \frac{\sin(\alpha_{\max}) p_\chi}{\cos(\gamma)\sqrt{p_\gamma^2 + \frac{p_\chi^2}{\cos^2(\gamma)}}} \ .$$

Since c_1 is always negative, we obtain $w_1 = \sqrt{1 - (w_2^2 + w_3^2)}$.

We analyze now the harder case $p_v^a|_J(\cdot) \neq 0$. Denote $\lambda = p_\gamma \omega$, $\rho = p_\chi \frac{\omega}{\cos(\gamma)}$. In the following, we apply the Karush-Kuhn-Tucker conditions. For this, we first remark that, if the constraints of (21) were active at the optimum, then it would satisfy $\boldsymbol{w} \in S^2$, $w_2^2 + w_3^2 = \sin^2(\alpha_{\max})$, and then, the gradients of the constraints evaluated at this point would satisfy the linear independence constraint qualification.

Applying the Karush-Kuhn-Tucker conditions to (21), we infer the existence of a non-zero multiplier $(\eta_1, \eta_2) \in \mathbb{R} \times \mathbb{R}_+$ which satisfies

$$\begin{cases} C_a - 2\eta_1 w_1 = 0 \quad , \quad 2(\eta_1 + \eta_2 + D_a) w_2 - \lambda = 0 \\ \\ 2(\eta_1 + \eta_2 + D_a) w_3 - \rho = 0 \ , \ \eta_2(w_2^2 + w_3^2 - \sin^2(\alpha_{\max})) = 0 \ . \end{cases}$$

Since either $\lambda \neq 0$ or $\rho \neq 0$, necessarily $\eta_1 + \eta_2 + D_a \neq 0$ and then the optimal control satisfies $\rho w_2 = \lambda w_3$. We proceed considering $\lambda \neq 0$, i.e. $w_3 = (\rho/\lambda) w_2$. The problem is reduced to the study of

$$\max \left\{ C_a w_1 - \left(1 + \frac{\rho^2}{\lambda^2}\right)(D_a w_2^2 - \lambda w_2) \ \mid \ w_1^2 + \left(1 + \frac{\rho^2}{\lambda^2}\right) w_2^2 = 1, \right.$$

$$\left. \left(1 + \frac{\rho^2}{\lambda^2}\right) w_2^2 \leq \sin^2(\alpha_{\max}) \right\} \ .$$

In other words, we seek points (w_1, w_2) such that the relations

$$w_1 = \frac{1}{C_a}\left(1+\frac{\rho^2}{\lambda^2}\right)(D_a w_2^2 - \lambda w_2) + \frac{C}{C_a}\ ,\ w_1^2 + \left(1+\frac{\rho^2}{\lambda^2}\right)w_2^2 = 1, \tag{37}$$

$$\left(1+\frac{\rho^2}{\lambda^2}\right)w_2^2 \leq \sin^2(\alpha_{\max})$$

are satisfied with the largest possible value of $C \in \mathbb{R}$. Several cases occur.

- $C_a > 0$:

  The optimum is given by the contact point between the parabola and the ellipse coming from (37), that lies in the positive half-plane $w_1 > 0$. Matching the first derivatives and using Assumption 2, we obtain

  $$w_1 = \sqrt{1 - \frac{\lambda^2+\rho^2}{(C_a+2D_a)^2}}\ ,\ w_2 = \frac{\lambda}{C_a+2D_a}$$

  if $\frac{\lambda^2+\rho^2}{(C_a+2D_a)^2} \leq \sin^2(\alpha_{\max})$. Saturations of the control may arise i.e., if $\frac{\lambda}{C_a+2D_a} < -\sin(\alpha_{\max})/(1+\frac{\rho^2}{\lambda^2})$, then $w_1 = \cos(\alpha_{\max})$, $w_2 = -\sin(\alpha_{\max})/(1+\frac{\rho^2}{\lambda^2})$ and, if $\frac{\lambda}{C_a+2D_a} > \sin(\alpha_{\max})/(1+\frac{\rho^2}{\lambda^2})$, then $w_1 = \cos(\alpha_{\max})$, $w_2 = \sin(\alpha_{\max})/(1+\frac{\rho^2}{\lambda^2})$.

- $C_a < 0$:

  In this case, since $w_1 > 0$, the optimum becomes the point of intersection beetwen the parabola and the upper part of the ellipse given by (37) for which C takes the maximum value. Only saturations are allowed. Indeed, if $\frac{\lambda}{C_a} > 0$, then $w_1 = \cos(\alpha_{\max})$, $w_2 = -\sin(\alpha_{\max})/(1+\frac{\rho^2}{\lambda^2})$ and, if $\frac{\lambda}{C_a} < 0$, then $w_1 = \cos(\alpha_{\max})$, $u_2 = \sin(\alpha_{\max})/(1+\frac{\rho^2}{\lambda^2})$.

A similar procedure holds when $\rho \neq 0$, $w_2 = (\lambda/\rho)w_3$.

At this step, we have found the optimal strategy in the regular case for the first local chart representation. By the similarity of (21) and (22), similar results hold true for the local control $\boldsymbol{z}$ using instead the second local chart (U_b, φ_b) for which λ and ρ are replaced respectively by $p_\theta\omega$ and by $-p_\phi\frac{\omega}{\cos(\theta)}$.

C. Computation of Singular Controls

In this section we compute singular optimal controls for (**GOGP**), under Assumption 1 and Assumption 3, within a non-zero mesure subset $J \subseteq [0, T]$. In the following, we need the adjoint

equations related to $(\mathbf{GOGP})_a$:

$$\begin{aligned}
\dot{p}_r^a &= p_L^a \frac{v}{r^2}\cos(\gamma)\cos(\chi) + p_l^a \frac{v}{r^2}\frac{\cos(\gamma)\sin(\chi)}{\cos(L)} \\
&+ p_\gamma\left(\frac{vc_m}{h_r}w_2 + \frac{v}{r^2}\cos(\gamma) + \frac{\partial g}{\partial r}\frac{\cos(\gamma)}{v}\right) \\
&+ p_\chi\left(\frac{vc_m}{h_r\cos(\gamma)}w_3 + \frac{v}{r^2}\cos(\gamma)\sin(\chi)\tan(L)\right) \\
&+ p_v^a\left(\frac{\partial g}{\partial r}\sin(\gamma) - \frac{v^2}{h_r}\big(d + \eta c_m(w_2^2 + w_3^2)\big)\right) \\
\dot{p^a}_L &= -p_l^a\frac{v}{r}\frac{\cos(\gamma)\sin(\chi)\tan(L)}{\cos(L)} - p_\chi\frac{v}{r}\frac{\cos(\gamma)\sin(\chi)}{\cos^2(L)} \\
\dot{p}_l^a &= 0
\end{aligned}$$

$$\begin{aligned}
\dot{p}_v^a &= -p_r^a\sin(\gamma) - p_L^a\frac{\cos(\gamma)\cos(\chi)}{r} - p_l^a\frac{\cos(\gamma)\sin(\chi)}{r\cos(L)} \\
&+ 2p_v^a v\big(d + \eta c_m(w_2^2 + w_3^2)\big) + p_\gamma\left(\frac{\omega}{v}w_2 - \frac{\cos(\gamma)}{r} - \frac{g}{v^2}\cos(\gamma)\right) \\
&+ p_\chi\left(\frac{\omega}{v}\frac{w_3}{\cos(\gamma)} - \frac{\cos(\gamma)\sin(\chi)\tan(L)}{r}\right)
\end{aligned}$$

$$\begin{aligned}
\dot{p}_\gamma &= -p_r^a v\cos(\gamma) + p_L^a\frac{v}{r}\sin(\gamma)\cos(\chi) + p_l^a\frac{v}{r}\frac{\sin(\gamma)\sin(\chi)}{\cos(L)} \\
&+ p_\chi\left(\frac{v}{r}\sin(\gamma)\sin(\chi)\tan(L) - \frac{\omega\sin(\gamma)}{\cos^2(\gamma)}w_3\right) \\
&+ p_\gamma\left(\frac{v}{r} - \frac{g}{v}\right)\sin(\gamma) + p_v^a g\cos(\gamma)
\end{aligned}$$

$$\dot{p}_\chi = p_L^a\frac{v}{r}\cos(\gamma)\sin(\chi) - p_l^a\frac{v}{r}\frac{\cos(\gamma)\cos(\chi)}{\cos(L)} - p_\chi\frac{v}{r}\cos(\gamma)\cos(\chi)\tan(L)$$

The first result is that, in the singular case, Assumption 1 allows to focus only on cases for which $p_v^a|_J(\cdot) \neq 0$ and $p_v^b|_J(\cdot) \neq 0$.

Lemma 1: Suppose $p_\gamma|_J(\cdot) = p_\chi|_J(\cdot) = 0$ (as well as $p_\theta|_J(\cdot) = p_\phi|_J(\cdot) = 0$). Then, under Assumption 1, $p_v^a|_J(\cdot) \neq 0$ (as well as $p_v^b|_J(\cdot) \neq 0$).

Proof: We prove the statement considering the first local chart (U_a, φ_a). The second local chart presents the same behavior. By contradiction, suppose that $p_\gamma|_J(\cdot) = p_\chi|_J(\cdot) = p_v^a|_J(\cdot) = 0$. From the adjoint equations of p_v^a, p_γ and p_χ restricted to J, we obtain

$$\begin{pmatrix} -v\cos(\gamma) & \frac{v}{r}\sin(\gamma)\cos(\chi) & \frac{v}{r}\frac{\sin(\gamma)\sin(\chi)}{\cos(L)} \\ 0 & \frac{v}{r}\cos(\gamma)\sin(\chi) & -\frac{v}{r}\frac{\cos(\gamma)\cos(\chi)}{\cos(L)} \\ -\sin(\gamma) & \frac{\cos(\gamma)\cos(\chi)}{r} & \frac{\cos(\gamma)\sin(\chi)}{r\cos(L)} \end{pmatrix} \begin{pmatrix} p_r^a \\ p_L^a \\ p_l^a \end{pmatrix} = \begin{pmatrix} 0 \\ 0 \\ 0 \end{pmatrix} .$$

The determinant of the matrix is $\frac{v^2\cos(\gamma)}{r^2\cos(L)} \neq 0$, then $(p_r^a, p_L^a, p_l^a)|_J(\cdot) = 0$. This implies that the adjoint vector is zero everywhere in $[0, T]$. Assumption 1, the transversality conditions and $\boldsymbol{p}(\cdot) \equiv 0$ give $p^0 = 0$, thus raising a contradiction because we must have $(\boldsymbol{p}(\cdot), p^0) \neq 0$. □

1) First Local Chart Representation: We start supposing that the system is described by using the first local chart (U_a, φ_a) in a non-zero mesure subset $J \subseteq [0, T]$. Then, we focus on (23). From now on $p_v^a|_J(\cdot) \neq 0$ and, when clear from the context, we skip the dependence on t to keep better readability. Moreover, we introduce the following local representation of the dynamical vectors

$$\begin{aligned} X(t, \boldsymbol{r}, \boldsymbol{v}) &:= v\sin(\gamma)\frac{\partial}{\partial r} + \frac{v}{r}\cos(\gamma)\cos(\chi)\frac{\partial}{\partial L} + \frac{v}{r}\frac{\cos(\gamma)\sin(\chi)}{\cos(L)}\frac{\partial}{\partial l} \\ &- \left(dv^2 + g\sin(\gamma)\right)\frac{\partial}{\partial v} + \left(\frac{v}{r} - \frac{g}{v}\right)\cos(\gamma)\frac{\partial}{\partial \gamma} + \frac{v}{r}\cos(\gamma)\sin(\chi)\tan(L)\frac{\partial}{\partial \chi} \\ Y_1(t, \boldsymbol{r}, \boldsymbol{v}) &:= \frac{f_T}{m}\frac{\partial}{\partial v} \quad , \quad Y_Q(t, \boldsymbol{r}, \boldsymbol{v}) := -\eta c_m v^2 \frac{\partial}{\partial v} \\ Y_2(t, \boldsymbol{r}, \boldsymbol{v}) &:= \omega\frac{\partial}{\partial \gamma} \quad , \quad Y_3(t, \boldsymbol{r}, \boldsymbol{v}) := \frac{\omega}{\cos(\gamma)}\frac{\partial}{\partial \chi} . \end{aligned}$$

We recall that the Lie bracket of two vector fields X, Y is defined as the derivation $[X, Y](f) := X(Yf) - Y(Xf)$, for every $f \in C^\infty$.

Lemma 2: Using the first local chart (U_a, φ_a), for times $t \in J$ such that $(\boldsymbol{r}, \boldsymbol{v})(t)$ lies within U_a, the following expressions hold:

$$\begin{aligned} \frac{d}{dt}\Big\langle \boldsymbol{p}, Y_2 \Big\rangle &= \Big\langle \boldsymbol{p}, \frac{\partial}{\partial t} Y_2 \Big\rangle + \Big\langle \boldsymbol{p}, [X, Y_2] \Big\rangle + w_1 \Big\langle \boldsymbol{p}, [Y_1, Y_2] \Big\rangle \\ &+ w_3 \Big\langle \boldsymbol{p}, [Y_3, Y_2] \Big\rangle + (w_2^2 + w_3^2) \Big\langle \boldsymbol{p}, [Y_Q, Y_2] \Big\rangle \end{aligned} \tag{38}$$

$$\frac{d}{dt}\Big\langle \boldsymbol{p}, Y_3\Big\rangle = \Big\langle \boldsymbol{p}, \frac{\partial}{\partial t} Y_3\Big\rangle + \Big\langle \boldsymbol{p}, [X, Y_3]\Big\rangle + w_1\Big\langle \boldsymbol{p}, [Y_1, Y_3]\Big\rangle \\ + w_2\Big\langle \boldsymbol{p}, [Y_2, Y_3]\Big\rangle + (w_2^2 + w_3^2)\Big\langle \boldsymbol{p}, [Y_Q, Y_3]\Big\rangle \tag{39}$$

$$\frac{d}{dt}\Big\langle \boldsymbol{p}, [X, Y_2]\Big\rangle = \Big\langle \boldsymbol{p}, \frac{\partial}{\partial t}[X, Y_2]\Big\rangle + \Big\langle \boldsymbol{p}, [X, [X, Y_2]]\Big\rangle \\ + w_1\Big\langle \boldsymbol{p}, [Y_1, [X, Y_2]]\Big\rangle + w_2\Big\langle \boldsymbol{p}, [Y_2, [X, Y_2]]\Big\rangle \\ + w_3\Big\langle \boldsymbol{p}, [Y_3, [X, Y_2]]\Big\rangle + (w_2^2 + w_3^2)\Big\langle \boldsymbol{p}, [Y_Q, [X, Y_2]]\Big\rangle \tag{40}$$

$$\frac{d}{dt}\Big\langle \boldsymbol{p}, [X, Y_3]\Big\rangle = \Big\langle \boldsymbol{p}, \frac{\partial}{\partial t}[X, Y_3]\Big\rangle + \Big\langle \boldsymbol{p}, [X, [X, Y_3]]\Big\rangle \\ + w_1\Big\langle \boldsymbol{p}, [Y_1, [X, Y_3]]\Big\rangle + w_2\Big\langle \boldsymbol{p}, [Y_2, [X, Y_3]]\Big\rangle \\ + w_3\Big\langle \boldsymbol{p}, [Y_3, [X, Y_3]]\Big\rangle + (w_2^2 + w_3^2)\Big\langle \boldsymbol{p}, [Y_Q, [X, Y_3]]\Big\rangle \ . \tag{41}$$

The idea developed here exploits expressions (38)-(41) to seek an analytical expression of the optimal control $\boldsymbol{w}(\cdot)$. The main step is based on the following statements which come from Lie bracket computations:

(A) $[Y_1, Y_2]$, $[Y_Q, Y_2]$ are proportional to $\frac{\partial}{\partial \gamma}$;

(B) $[Y_1, Y_3]$, $[Y_2, Y_3]$, $[Y_Q, Y_3]$, $[Y_2, [X, Y_3]]$ are proportional to $\frac{\partial}{\partial \chi}$;

(C) Considering $p_\gamma|_J(\cdot) = p_\chi|_J(\cdot) = 0$, then $\big\langle \boldsymbol{p}, [X, [X, Y_3]]\big\rangle$, $\big\langle \boldsymbol{p}, [Y_1, [X, Y_3]]\big\rangle$, $\big\langle \boldsymbol{p}, [Y_Q, [X, Y_3]]\big\rangle$ are proportional to $\dot{p}_\chi$;

(D) Considering $p_\gamma|_J(\cdot) = p_\chi|_J(\cdot) = 0$, then $\big\langle \boldsymbol{p}, \frac{\partial}{\partial t}[X, Y_2]\big\rangle$ is proportional to $\big\langle \boldsymbol{p}, [X, Y_2]\big\rangle$ while $\big\langle \boldsymbol{p}, \frac{\partial}{\partial t}[X, Y_3]\big\rangle$ is proportional to $\big\langle \boldsymbol{p}, [X, Y_3]\big\rangle$.

Now, $p_\gamma|_J(\cdot) = p_\chi|_J(\cdot) = 0$ holds. Then, (A) and (B) applied to (38) and (39) give $\Big\langle \boldsymbol{p}, [X, Y_2]\Big\rangle\Big|_J = \Big\langle \boldsymbol{p}, [X, Y_3]\Big\rangle\Big|_J = 0$. These expressions, plugged into (41) using (B), (C) and (D), lead to

$$w_3 \cdot \Big\langle \boldsymbol{p}, [Y_3, [X, Y_3]]\Big\rangle = 0 \ , \ \text{in } J \ . \tag{42}$$

Seeking an analytical expression of the singular control from (42) becomes a hard and tedious task if $\Big\langle \boldsymbol{p}, [Y_3, [X, Y_3]]\Big\rangle = 0$ because more many time derivatives are required. Fortunately, the physical environment of general lunch vehicle applications help us making these time derivative computations useless.

Lemma 3: Under Assumption 3, $\Big\langle \boldsymbol{p}, [Y_3, [X, Y_3]]\Big\rangle \neq 0$ almost everywhere in J.

Proof: By contradiction, suppose that $\Big\langle \boldsymbol{p}, [Y_3, [X, Y_3]] \Big\rangle = 0$ a.e. within J. This implies that $\cos(\chi) p_L^a + \frac{\sin(\chi)}{\cos(L)} p_l^a = 0$ a.e. within J. The previous expression, combined with the adjoint equation of p_χ, gives $p_L^a|_J(\cdot) = p_l^a|_J(\cdot) = 0$.

On the other hand, from the adjoint equation of p_γ, we have $(v p_r^a - g p_v^a)|_J(\cdot) = 0$. Combining this expression with its derivative w.r.t. time within J and imposing $p_v^a|_J(\cdot) \neq 0$ lead to

$$v^4 + 3g(\boldsymbol{r}) h_r v^2 - g(\boldsymbol{r}) h_r \left(\frac{f_T w_1}{m(d + \eta c_m (w_2^2 + w_3^2))} \right) = 0 \ .$$

First of all, if $f_T = 0$ a contradiction arises immediately. The only physically meaningful solution is

$$v = \sqrt{\frac{3}{2} g(\boldsymbol{r}) h_r} \sqrt{\sqrt{1 + \frac{4}{9} \frac{1}{g(\boldsymbol{r}) h_r} \left(\frac{f_T w_1}{m(d + \eta c_m (w_2^2 + w_3^2))} \right)} - 1}$$

and, since $0 \leq w_1 \leq 1$, a contradiction arises because of Assumption 3. □

The previous results make us able to reformulate (23) as

$$(w_1, w_2) = \text{argmax} \Big\{ C_a w_1 - D_a w_2^2 \ \mid \ w_1^2 + w_2^2 = 1 \ , \ w_2^2 \leq \sin^2(\alpha_{\max}) \Big\}$$

that, now, we can solve. Notice that $D_a \neq 0$ and $C_a \neq 0$ if and only if $f_T \neq 0$.

Suppose first that $C_a = 0$ (i.e. the system crosses a ballistic phase). In this case, it is clear that component w_1 of the control does not affect the dynamics and then we can chose it arbitrarily, satisfying the appropriate constraints. For this, we obtain $w_1 = 1$, $w_2 = 0$ if $D_a > 0$ and $w_1 = \cos(\alpha_{\max})$, $w_2^2 = \sin^2(\alpha_{\max})$ if $D_a < 0$.

Let now $C_a \neq 0$. Exploiting a graphical study, it is clear that $w_1 = 1$, $w_2 = 0$ if $C_a > 0$ while $w_1 = \cos(\alpha_{\max})$, $w_2^2 = \sin^2(\alpha_{\max})$ if $C_a < 0$.

To conclude the study of the optimal control w.r.t. the first local chart, it remains to establish the value of the coordinate w_2 when $w_1 = \cos(\alpha_{\max})$ and $w_2^2 = \sin^2(\alpha_{\max})$. For this, we recall expression (40). Indeed, it is clear that, when $\Big\langle \boldsymbol{p}, [Y_2, [X, Y_2]] \Big\rangle \neq 0$, the second coordinate of the control is given by (recall statements (A)-(D))

$$w_2 = -\frac{\Big\langle \boldsymbol{p}, [X, [X, Y_2]] \Big\rangle}{\Big\langle \boldsymbol{p}, [Y_2, [X, Y_2]] \Big\rangle} - w_1 \frac{\Big\langle \boldsymbol{p}, [Y_1, [X, Y_2]] \Big\rangle}{\Big\langle \boldsymbol{p}, [Y_2, [X, Y_2]] \Big\rangle}$$
$$- w_2^2 \frac{\Big\langle \boldsymbol{p}, [Y_Q, [X, Y_2]] \Big\rangle}{\Big\langle \boldsymbol{p}, [Y_2, [X, Y_2]] \Big\rangle} \quad .$$

If instead $\Big\langle \boldsymbol{p}, [Y_2,[X,Y_2]] \Big\rangle = 0$ a.e. in J, then, suppose that $\Big\langle \boldsymbol{p}, [Y_2,[Y_2,[X,Y_2]]] \Big\rangle \neq 0$. Proceeding as in (40), (41) with the same arguments as above, we have

$$w_2 = -\frac{\Big\langle \boldsymbol{p}, [Y_2,[X,[X,Y_2]]] \Big\rangle}{\Big\langle \boldsymbol{p}, [Y_2,[Y_2,[X,Y_2]]] \Big\rangle} - w_1 \frac{\Big\langle \boldsymbol{p}, [Y_2,[Y_1,[X,Y_2]]] \Big\rangle}{\Big\langle \boldsymbol{p}, [Y_2,[Y_2,[X,Y_2]]] \Big\rangle}$$
$$-w_2^2 \frac{\Big\langle \boldsymbol{p}, [Y_2,[Y_Q,[X,Y_2]]] \Big\rangle}{\Big\langle \boldsymbol{p}, [Y_2,[Y_2,[X,Y_2]]] \Big\rangle} \quad .$$

We can prove that actually one between the two previous formulas always holds.

Lemma 4: Under Assumption 3, almost everywhere in J, it holds

$$\Big\langle \boldsymbol{p}, [Y_2,[X,Y_2]] \Big\rangle \neq 0 \quad \text{or} \quad \Big\langle \boldsymbol{p}, [Y_2,[Y_2,[X,Y_2]]] \Big\rangle \neq 0 \ .$$

Proof: By contradiction, $\Big\langle \boldsymbol{p}, [Y_2,[X,Y_2]] \Big\rangle = 0$ and $\Big\langle \boldsymbol{p}, [Y_2,[Y_2,[X,Y_2]]] \Big\rangle = 0$ a.e. in J. From this, one recovers respectively the following two expressions

$$\left(\sin(\gamma) p_r^a + \frac{\cos(\gamma)\cos(\chi)}{r} p_L^a + \frac{\cos(\gamma)\sin(\chi)}{r\cos(L)} p_l^a - vg\sin(\gamma) p_v^a \right)\Big|_J (\cdot) = 0$$
$$\left(\cos(\gamma) p_r^a - \frac{\sin(\gamma)\cos(\chi)}{r} p_L^a - \frac{\sin(\gamma)\sin(\chi)}{r\cos(L)} p_l^a - vg\cos(\gamma) p_v^a \right)\Big|_J (\cdot) = 0$$

which lead to $\cos(\chi) p_L^a + \frac{\sin(\chi)}{\cos(L)} p_l^a = 0$ a.e. within J. This expression, combined with the adjoint equation of p_χ, gives $p_L^a|_J(\cdot) = p_l^a|_J(\cdot) = 0$. On the other hand, from the adjoint equation of p_γ, we have $(vp_r^a - gp_v^a)|_J(\cdot) = 0$. Proceeding as in the proof of Lemma 3, a contradiction arises. □

2) Second Local Chart Representation: The approach proposed in the previous section is no more exploitable in the second local chart (U_b, φ_b) for (24). Indeed, the terms of the gravity and the curvature of the Earth contained in (19) make the computations on the Lie algebra generated by the local fields hard to treat. However, we can still recover singular arcs.

Thanks to the previous computation, we know the analytical behavior of singular controls for every point of the domain of the first local chart. Then, it is enough to compute possible singular arcs at points of the domain of the second local chart that do not belong to the domain of the first one. From (11) and (16), one sees that these points lie exactly within the following four-dimensional submanifold of $\mathbb{R}^6 \setminus \{0\}$

$$S_a := \big\{ (\boldsymbol{r}, \boldsymbol{v}) \in \mathbb{R}^6 \setminus \{0\} \ \mid \ \boldsymbol{v} \ /\!\!/ \ \boldsymbol{r} \big\}$$

and which corresponds, in the (extended) coordinates of the chart (U_b, φ_b), to points such that $\theta = 0$, $\phi = 0$ or $\theta = 0$, $\phi = \pi$. Following the previous argument, suppose that there exists a non-zero measure subset $J \subseteq [0, T]$ such that the optimal trajectory $(\boldsymbol{r}, \boldsymbol{v})(\cdot)$ arisen from a singular control $\boldsymbol{u}(\cdot)$ is such that $(\boldsymbol{r}, \boldsymbol{v})(t) \in S_a$ for every $t \in J$. In particular, suppose that $\theta|_J(\cdot) = 0$, $\phi|_J(\cdot) = 0$ or $\phi|_J(\cdot) = \pi$. Then, almost everywhere in J, $(\boldsymbol{r}, \boldsymbol{v})(\cdot)$ satisfies

$$\begin{cases} \dot{r} = -v \ , \ \dot{L} = 0 \ , \ \dot{l} = 0 \ , \ \dot{\theta} = \omega z_2 \ , \ \dot{\phi} = -\omega z_3 \\ \dot{v} = \dfrac{f_T}{m} z_1 - \left(d + \eta c_m (z_2^2 + z_3^2)\right) v^2 \pm g \qquad . \end{cases}$$

Since the values of θ and ϕ remain the same along J, their derivative w.r.t. the time must be zero. Therefore, almost everywhere in J, the singular control satisfies $z_1|_J(\cdot) = 1$, $z_2|_J(\cdot) = 0$ and $z_3|_J(\cdot) = 0$, which concludes the analysis.

REFERENCES

[1] Eugene L Allgower and Kurt Georg. *Introduction to numerical continuation methods*, volume 45. SIAM, 2003.

[2] Aram V Arutyunov, D Yu Karamzin, and Fernando Lobo Pereira. The maximum principle for optimal control problems with state constraints by gamkrelidze: revisited. *Journal of Optimization Theory and Applications*, 149(3):474–493, 2011.

[3] Mark J Balas. Adaptive control of nonminimum phase systems using sensor blending with application to launch vehicle control. In *Conference on Smart Materials, Adaptive Structures and Intelligent Systems. Stone Mountain*, 2012.

[4] Riccardo Bonalli, Bruno Hérissé, and Emmanuel Trélat. Analytical initialization of a continuation-based indirect method for optimal control of endo-atmospheric launch vehicle systems. In *2017 IFAC World Congress, IFAC 2017, Toulouse, France, July 9-14, 2017*.

[5] Riccardo Bonalli, Bruno Hérissé, and Emmanuel Trélat. Solving optimal control problems for delayed control-affine systems with quadratic cost by numerical continuation. In *2017 American Control Conference, ACC 2017, Seattle, WA, USA, May 24-26, 2017*, pages 649–654, 2017.

[6] J Frédéric Bonnans and Audrey Hermant. Well-posedness of the shooting algorithm for state constrained optimal control problems with a single constraint and control. *SIAM Journal on Control and Optimization*, 46(4):1398–1430, 2007.

[7] Bernard Bonnard, Ludovic Faubourg, Genevieve Launay, and Emmanuel Trélat. Optimal control with state constraints and the space shuttle re-entry problem. *Journal of Dynamical and Control Systems*, 9(2):155–199, 2003.

[8] Arthur Earl Bryson. *Applied optimal control: optimization, estimation and control*. CRC Press, 1975.

[9] J-B Caillau, Olivier Cots, and Joseph Gergaud. Differential continuation for regular optimal control problems. *Optimization Methods and Software*, 27(2):177–196, 2012.

[10] A Calise. A singular perturbation analysis of optimal aerodynamic and thrust magnitude control. *IEEE Transactions on Automatic Control*, 24(5):720–730, 1979.

[11] Anthony J Calise, Nahum Melamed, and Seungjae Lee. Design and evaluation of a three-dimensional optimal ascent guidance algorithm. *Journal of Guidance Control and Dynamics*, 21:867–875, 1998.

[12] Max Cerf, Thomas Haberkorn, and Emmanuel Trélat. Continuation from a flat to a round earth model in the coplanar orbit transfer problem. *Optimal Control Applications and Methods*, 33(6):654–675, 2012.

[13] Francis Clarke and MDR De Pinho. Optimal control problems with mixed constraints. *SIAM Journal on Control and Optimization*, 48(7):4500–4524, 2010.

[14] Ronald G Cottrell. Optimal intercept guidance for short-range tactical missiles. *AIAA journal*, 9(7):1414–1415, 1971.

[15] MDR De Pinho, RB Vinter, and H Zheng. A maximum principle for optimal control problems with mixed constraints. *IMA Journal of Mathematical Control and Information*, 18(2):189–205, 2001.

[16] J.J. Moré et al. The minpack project. In *Sources and Development of Mathematical Software*, pages 88–111. Prentice-Hall, Englewood Cliffs, NJ, 1984.

[17] Robert Fourer, David M Gay, and Brian Kernighan. *Ampl*, volume 117. Boyd & Fraser Danvers, MA, 1993.

[18] Knut Graichen and Nicolas Petit. A continuation approach to state and adjoint calculation in optimal control applied to the reentry problem. *IFAC Proceedings Volumes*, 41(2):14307–14312, 2008.

[19] Charles R Hargraves and Stephen W Paris. Direct trajectory optimization using nonlinear programming and collocation. *Journal of Guidance, Control, and Dynamics*, 10(4):338–342, 1987.

[20] Richard F Hartl, Suresh P Sethi, and Raymond G Vickson. A survey of the maximum principles for optimal control problems with state constraints. *SIAM review*, 37(2):181–218, 1995.

[21] Magnus Rudolph Hestenes. Calculus of variations and optimal control theory. 1965.

[22] Nahshon Indig, Joseph Z Ben-Asher, and Nathan Farber. Near-optimal spatial midcourse guidance law with an angular constraint. *Journal of Guidance, Control, and Dynamics*, 37(1):214–223, 2013.

[23] David H Jacobson, Milind M Lele, and Jason L Speyer. New necessary conditions of optimality for control problems with state-variable inequality constraints. *Journal of mathematical analysis and applications*, 35(2):255–284, 1971.

[24] Ernest Bruce Lee and Lawrence Markus. Foundations of optimal control theory. Technical report, DTIC Document, 1967.

[25] CF Lin and L Tsai. Analytical solution of optimal trajectory-shaping guidance. *Journal of Guidance, Control, and Dynamics*, 10(1):60–66, 1987.

[26] Ching-Fang Lin. *Modern navigation, guidance, and control processing*, volume 2. Prentice Hall Englewood Cliffs, 1991.

[27] Ping Lu, Hongsheng Sun, and Bruce Tsai. Closed-loop endoatmospheric ascent guidance. *Journal of Guidance, Control, and Dynamics*, 26(2):283–294, 2003.

[28] Helmut Maurer. On optimal control problems with bounded state variables and control appearing linearly. *SIAM Journal on Control and Optimization*, 15(3):345–362, 1977.

[29] Robert Wes Morgan, Hal Tharp, and Thomas L Vincent. Minimum energy guidance for aerodynamically controlled missiles. *IEEE Transactions on Automatic Control*, 56(9):2026–2037, 2011.

[30] Binfeng Pan and Ping Lu. Improvements to optimal launch ascent guidance. *AIAA Paper*, 8174:2, 2010.

[31] Christopher Petersen, Morgan Baldwin, and Ilya Kolmanovsky. Model predictive control guidance with extended command governor inner-loop flight control for hypersonic vehicles. *AIAA Guidance, Navigation and Control, Boston, USA*, 2013.

[32] Mauro Pontani and Giampaolo Cecchetti. Ascent trajectories of multistage launch vehicles: Numerical optimization with second-order conditions verification. *ISRN Operations Research*, 2013, 2013.

[33] Lev Semenovich Pontryagin. *Mathematical theory of optimal processes*. CRC Press, 1987.

[34] Daniele Pucci, Tarek Hamel, Pascal Morin, and Claude Samson. Nonlinear feedback control of axisymmetric aerial vehicles. *Automatica*, 53:72–78, 2015.

[35] I Michael Ross and Fariba Fahroo. A direct method for solving nonsmooth optimal control problems. *IFAC Proceedings Volumes*, 35(1):479–484, 2002.

[36] Isaac M Ross, Christopher DSouza, Fariba Fahroo, and JB Ross. A fast approach to multi-stage launch vehicle trajectory optimization. In *aiaa Guidance, Navigation, and control conference and Exhibit*, volume 11, page 14, 2003.

[37] J Shinar and I Forte. On the optimal pure strategy sets for a mixed missile guidance law synthesis. *IEEE Transactions on Automatic Control*, 36(11):1296–1300, 1991.

[38] Emmanuel Trélat. Optimal control and applications to aerospace: some results and challenges. *Journal of Optimization Theory and Applications*, 154(3):713–758, 2012.

[39] Avishai Weiss, Morgan Baldwin, Richard Scott Erwin, and Ilya Kolmanovsky. Model predictive control for spacecraft rendezvous and docking: Strategies for handling constraints and case studies. *IEEE Transactions on Control Systems Technology*, 23(4):1638–1647, 2015.

[40] Jiamin Zhu, Emmanuel Trélat, and Max Cerf. Minimum time control of the rocket attitude reorientation associated with orbit dynamics. *SIAM Journal on Control and Optimization*, 54(1):391–422, 2016.

[41] Jiamin Zhu, Emmanuel Trélat, and Max Cerf. Planar tilting maneuver of a spacecraft: singular arcs in the minimum time problem and chattering. *Discrete and Continuous Dynamical Systems-Series B*, 16(4):1347–1388, 2016.

Riccardo Bonalli obtained his MSc System Engineering and Numerical Mathematics from Politecnico di Milano, Italy, in 2014. He is currently pursuing the Ph.D. degree at ONERA - The French Aerospace Lab, Palaiseau, France, and at University Pierre et Marie Curie, Paris, France. His main research interests concern the theoretical and numerical optimal control with applications in aerospace engineering.

Bruno Hérissé received the Engineering degree and the Master degree from the École Supérieure d'Électricité (SUPELEC), Paris, France, in 2007. After three years of research with CEA List, he received the Ph.D. degree in robotics from the University of Nice Sophia Antipolis, Sophia Antipolis, France, in 2010. Since 2011, he has been a Research Engineer with ONERA, the French Aerospace Lab, Palaiseau, France. His research interests include optimal control and vision-based control with applications in aerospace sytems and aerial robotics.

Emmanuel Trélat was born in 1974. He is currently full professor at University Pierre et Marie Curie (Paris 6). He is the director of the Fondation Sciences Mathématiques de Paris. He is editor in chief of the journal ESAIM: Control Calculus of Variations and Optimization, and is associated editor of many other journals. He has been awarded the SIAM Outstanding Paper Prize (2006), Maurice Audin Prize (2010), Felix Klein Prize (European Math. Society, 2012), Blaise Pascal Prize (french Academy of Science, 2014), Big Prize Victor Noury (french Academy of Science, 2016). His research interests range over control theory in finite and infinite dimension, optimal control, stabilization, geometry, numerical analysis, with a special interest to applications of optimal control to aerospace.